GEOSPHERE

GEOSPHERE, v. 17

https://doi.org/10.1130/GES02305.1

14 figures; 1 table

CORRESPONDENCE: gmoore@hawaii.edu

CITATION: Tilley, H.L., Moore, G.F., Yamashita, M., and Kodaira, S., 2021, Along-strike variations in prothrust zone characteristics at the Nankai Trough subduction margin: Geosphere, v. 17, https://doi.org/10.1130/GES02305.1.

Science Editor: Shanaka de Silva
Guest Associate Editor: David W. Scholl

Received 22 June 2020
Revision received 5 October 2020
Accepted 9 December 2020

Along-strike variations in prothrust zone characteristics at the Nankai Trough subduction margin

Hannah L. Tilley[1], Gregory F. Moore[1], Mikiya Yamashita[2,*], and Shuichi Kodaira[2]

[1]Department of Earth Sciences, University of Hawai'i at Manoa, 1630 East-West Road, Honolulu, Hawaii 96822, USA
[2]Japan Agency for Marine-Earth Science and Technology, 3173-25 Showa-Machi, Kanazawa-ku, Yokohama 236-0001, Japan

ABSTRACT

Significant along-strike changes in the prothrust zone at the toe of the Nankai Trough accretionary prism were imaged in new high-resolution seismic reflection data. The width of the prothrust zone varies greatly along strike; two spatially discrete segments have a wide prothrust zone (~3.3–7.8 km, ~50–110 prothrusts), and two segments have almost no prothrust zone (~0.5–2.8 km, <20 prothrusts). The widest prothrust zone occurs in the region with the widest and thickest sediment wedge and subducting turbidite package, both of which are influenced by basement topography. The trench wedge size and lithology, the lithology of the subducting section, and the basement topography all influence the rate of consolidation in the trench wedge, which we hypothesize is an important control over the presence and width of the prothrust zone. We conclude that prothrusts are fractures that form from shear surfaces in deformation band clusters as the trench fill sediment is consolidated. Strain localization occurs at sites with a high density of prothrusts, which become the probable locations of future frontal thrust propagation. The frontal thrust may propagate forward with a lower buildup of strain where it is adjacent to a wide prothrust zone than at areas with a narrow or no prothrust zone. This is reflected in the accretionary prism geometry, where wide prothrust zones occur adjacent to fault-propagation folds with shallow prism toe surface slopes.

INTRODUCTION

Convergent margins host a wide range of deformation processes that vary greatly both between different margins as well as along individual margins. In some cases, a prothrust zone extends seaward from the frontal thrust to the deformation front, which is the furthest seaward expression of faulting. The prothrust zone is an area with parallel shear structures that have relatively small offsets (e.g., Nankai Trough—Karig, 1986; Cascadia—Wang et al., 1994; Hikurangi—Barnes et al., 2018). However, prothrust zones only occur in discrete locations, and it is unclear how they relate to other subduction zone characteristics. The Nankai Trough subduction zone in SW Japan (Fig. 1) is one of the few places where prothrusts are well developed. It has also been the site of many geological and geophysical surveys in the last few decades, making it an ideal laboratory for studying the relationship between prothrusts and other subduction margin characteristics (e.g., Taira et al., 1991; Moran et al., 1993; Bangs et al., 2004; Yamashita et al., 2018). Drill cores at Ocean Drilling Program (ODP) Site 1174 (landward of the deformation front) revealed deformation bands in the Nankai prothrust zone that were interpreted to correlate with the prothrusts in seismic images (Karig and Lundberg, 1990; Ujiie et al., 2004). However, the relationship between core-scale deformation bands and seismic-scale features in the prothrust zone is poorly understood. As

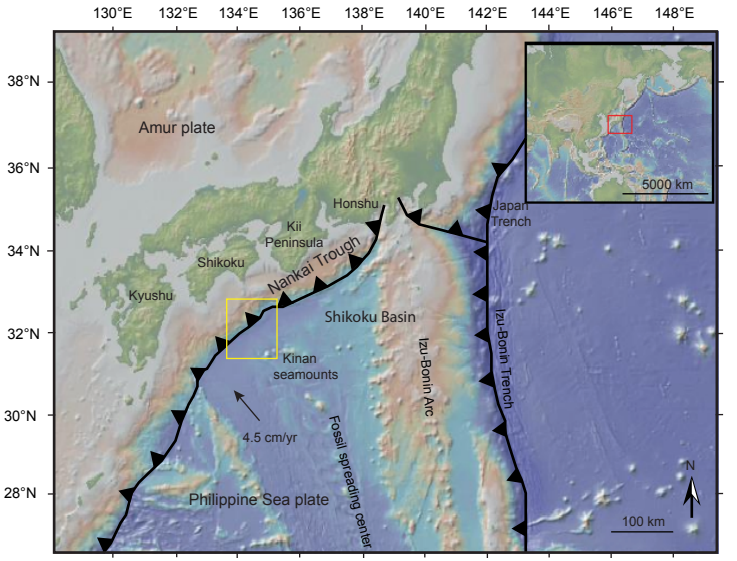

Figure 1. Tectonic map of the Nankai Trough. Yellow box outlines the study area shown in Figure 2. Arrow shows the convergence direction of the Philippine Sea plate beneath Japan. Inset shows the location of the Nankai Trough in East Asia.

Gregory Moore https://orcid.org/0000-0002-9649-3174
*Now at Geological Survey of Japan, National Institute of Advanced Industrial Science and Technology (AIST), Tsukuba Central 7, 1-1-1 Higashi, Tsukuba, Ibaraki, 305-8567, Japan

a result, the nature of protothrusts and the physical conditions that promote their formation have not been well established.

Karig and Lundberg (1990) suggested that protothrusts are narrow panels of slightly steeper-dipping beds that host deformation bands and that deformation bands initially form at shallower angles in subhorizontal beds but are rotated to steeper dips within these panels. Deformation bands can include compaction bands, shear bands, and dilation bands or hybrids of these bands (Karig and Lundberg, 1990; Bésuelle, 2001). The specific deformation mechanism depends on the mineralogy, grain size and shape, sorting, cementation, porosity, and stress state of the sediment (Fossen et al., 2007). However, deformation bands form preferentially in coarser, high-porosity sediment (Fossen et al., 2018), which is commonly found at accretionary margin trench wedges.

The evidence for the steeper-dipping panels comes from cores that show localized bedding dips of 10°–15°, which do not agree with the shallow dips in seismic sections. These dips led Morgan et al. (1994) to postulate that the protothrusts could represent narrow angular folds caused by local buckling.

Lateral variations in the incoming crust and the overlying sediment type and thickness are thought to control along-strike variations in the Nankai Trough accretionary prism. However, the relationship between the incoming material and the deformation processes is still poorly understood. This study addressed the role of subducting topography and sediment properties in producing variations in the accretionary prism along the Nankai Trough subduction zone by examining the protothrust zone. We investigated how the protothrust zone is affected by changes in the incoming plate and sediment, as well as how protothrusts develop from deformation bands into the frontal thrust. We also considered how protothrust zones are related to the style of frontal thrust propagation. We used high-resolution seismic reflection data that cover a wide section of the margin to infer that variations in the protothrust zone are caused by variations in the incoming sediment, which in turn influence strain localization of the sediment and thus its behavior during accretion.

REGIONAL SETTING

Tectonic History

The heterogeneous basement structure of the subducting Shikoku Basin (Kobayashi et al., 1995) and its highly variable sediment cover (Ike et al., 2008) strongly influence deformation at the Nankai Trough. The Shikoku Basin lithosphere was formed during back-arc rifting and seafloor spreading in the eastern part of the Philippine Sea plate between 30 and 15 Ma (Watts and Weissel, 1975; Kobayashi and Nakada, 1978; Taylor and Fujioka, 1992; Okino et al., 1994; Sdrolias et al., 2004). The extinct Shikoku Basin spreading center lies just to the east of our study area, so the age of the basin increases to the SW. The Kinan seamount chain (Fig. 1), which trends roughly NNW-SSE down the center of the basin, formed near the extinct spreading axis. Although organized spreading ceased ca. 15 Ma, seamount eruptions continued to as recently as 8–7 Ma (Ishii, 2000; Sato et al., 2002; Ishizuka et al., 2009). The superposition of seamount topography on the subducting Shikoku Basin topography has had profound effects on the structure of the Nankai accretionary prism.

An important event in the history of the Shikoku Basin that greatly affected the sedimentation patterns in the basin was the apparent cessation of subduction at the Nankai Trough at ca. 12 Ma, followed by resurgence of subduction at ca. 6 Ma (Kimura et al., 2014, 2018; Wu et al., 2016). During this gap in subduction, sediment delivered from the Japanese Islands flooded the trench and poured far out onto the floor of Shikoku Basin (e.g., Pickering et al., 2013). Subsequent reinitiation of subduction after ca. 6 Ma led to the formation of the bathymetric low that defines the present Nankai Trough. Collision of the Izu-Bonin arc with Honshu and convergence between SW Japan and NE Japan at ca. 2 Ma caused uplift in eastern Honshu that supplied sediments to the trough through submarine canyon systems (Kimura et al., 2018).

Sedimentation History

The large variations in basement relief of the subducting Philippine Sea plate have resulted in variations in overlying sediment thickness and type. Few of the regional and local variations in basement topography are reflected in the seafloor bathymetry because the basement topography is almost completely buried beneath the sediment. Our seismic-stratigraphic interpretations were based on core-log-seismic correlations at several Deep Sea Drilling Project (DSDP), ODP, and Integrated Ocean Drilling Program (IODP) sites (Fig. 2). We followed the facies designations defined by Underwood and Pickering (2018), who used core data from the IODP Kumano transect (Underwood et al., 2010) to redefine the earlier facies terminology, which was based on results from previous ODP drilling on Legs 131 and 190 (e.g., Ike et al., 2008).

The oldest stratigraphic unit is a volcaniclastic facies that overlies the oceanic basement. It is much thicker at the western ODP Site 1177 along the Ashizuri (western) transect than in the Muroto (eastern) transect (Fig. 2; ODP Sites 808, 1173, and 1174; Moore et al., 2001; Steurer and Underwood, 2003). This facies also has a higher proportion of siliciclastic silt at Site 1177 than at Site 1173. Overlying the basal volcaniclastic unit at Site 1177, there is a package of siliciclastic turbidites with abundant organic matter. These are interpreted to be Lower to Middle Miocene Kyushu Fan deposits (LSB-T of Ike et al., 2008), which were supplied by a mainland source area, possibly between Kyushu and Shikoku, and transported along a westerly supply route (Pickering et al., 2013). These deposits are not present at Site 1173 (Underwood, 2007) due to the deflection of turbidity current flow paths around the Kinan seamount chain.

The Shikoku Basin facies consists of hemipelagic and pyroclastic/hemipelagic mudstones with ages of 12.5–9.1 Ma and 7.8 Ma–recent, respectively (Underwood and Pickering, 2018; Upper Shikoku Basin [USB] and

Lower Shikoku Basin [LSB] of Ike et al., 2008). The USB/LSB boundary is diagenetic, and we refer to it as the "diagenetic boundary." The pyroclastic/hemipelagic–hemipelagic boundary is lithological and was identified in drill cores as the onset of ash beds. The mudstones in the western Shikoku Basin contain a higher percentage of smectite than those in the central Shikoku Basin (Steurer and Underwood, 2003). Additionally, the cessation of near-trench volcanism ca. 11 Ma (Kimura et al., 2005) resulted in a gradual change from smectite- to illite-dominated clay mineral assemblages (Underwood and Fergusson, 2005; Guo and Underwood, 2011). This temporal change in mineralogy supports a mainland terrigenous source, even though the Izu-Bonin arc was closer to the eastern part of the basin during the Miocene (Underwood et al., 2010). Significant lateral transport of volcanic lithic sediment along the trough axis from the Izu-Honshu collision zone during the Quaternary led to the development of the axial trench sediment wedge on top of the older Shikoku Basin deposits (e.g., Underwood and Fergusson, 2005; Underwood and Pickering, 2018).

DATA ACQUISITION AND PROCESSING

Seventeen two-dimensional (2-D) high-resolution seismic reflection lines were collected across the Nankai Trough trench axis (Fig. 3) on the R/V *Kaiyo* of the Japan Agency for Marine-Earth Science and Technology (JAMSTEC) in 2013 (KY13–11) and 2014 (KY14–07). For high-resolution shallow seismic imaging, a 380 in.^{3} (6.23 L) air-gun array was used with a 1.2-km-long hydrophone streamer that had 192 channels at a 6.25 m interval. Standard seismic processing techniques were applied, including noisy trace editing, 20–200 Hz band-pass filtering, normal move-out (NMO) correction, 16-fold common midpoint (CMP) binning with a 3.125 m interval, stack, and Kirchhoff time migration. We then performed time-to-depth conversion using velocity functions based on a three-dimensional (3-D) P-wave velocity model derived from the JAMSTEC regional ocean-bottom seismometer (OBS) surveys (Nakanishi et al., 2018). Observations of along-strike variations in sediment properties and oceanic basement relief were supplemented by several longer-offset 2-D seismic surveys (e.g., Moore et al., 1990, 2001; Ike et al., 2008;

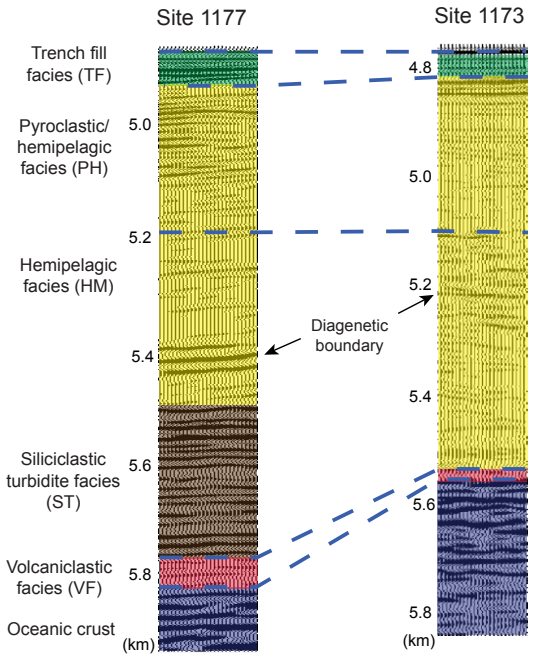

Figure 2. Seismic stratigraphy of Ocean Drilling Program (ODP) cores at Sites 1177 (western Nankai) and 1173 (central Nankai). Site 1177 has siliciclastic turbidites (ST), which do not occur at Site 1173. The locations of the cores are projected onto the cross line (Fig. 4) and strike lines (Figs. 7 and 10) perpendicular to local structural trends.

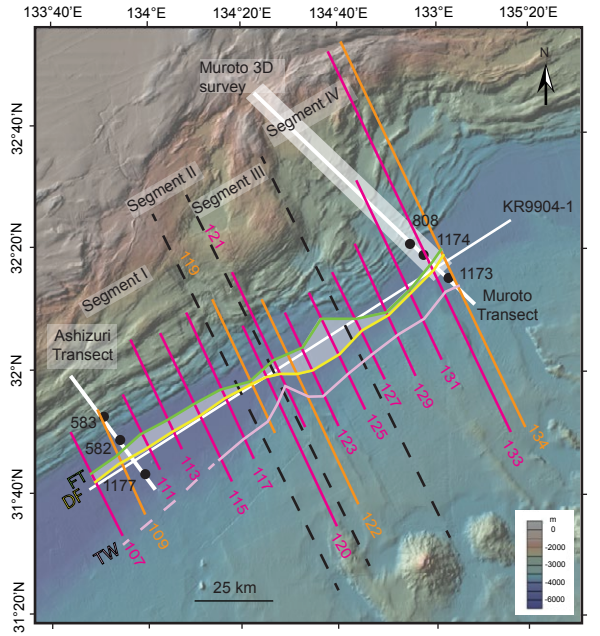

Figure 3. High-resolution two-dimensional (2-D) seismic lines (magenta) and previous 2-D and three-dimensional (3-D) seismic surveys (white) in the Nankai Trough. Orange lines are high-resolution lines used in Figures 7–10. Ocean Drilling Program (ODP)/Deep Sea Drilling Project (DSDP) drill sites are marked as black circles. Locations of the frontal thrust (FT, green), deformation front (DF, yellow), and trench wedge (TW, lilac) were interpolated between each seismic line.

Park et al., 2014) that were oriented both parallel and perpendicular to the protothrust zone, as well as the Muroto transect 3-D survey (Fig. 3; Bangs et al., 2004).

SEISMIC INTERPRETATION

Seismic Stratigraphy

The deepest mapped unit is the volcaniclastic facies, which overlies the oceanic crust. The Kyushu Fan siliciclastic turbidite sequence, the next oldest mapped unit (Fig. 2), is characterized by continuous, parallel-bedded, high-amplitude reflections. The sequence is not ubiquitous along strike but instead occurs mostly in basement lows (e.g., Fig. 4), and it onlaps the basement topography, most notably the basement scarp in lines 121–123 (Fig. 5). The siliciclastic turbidite package is continuous along lines 107–117, where the basement is smooth with small variations in topography (<150 m; Figs. 4 and 5). There is a thin siliciclastic turbidite package along lines 121–125, although it has fewer distinct layers than the siliciclastic turbidite package along lines 107–117. Along line 127, there is a siliciclastic turbidite package seaward of the frontal thrust, which onlaps a basement high at its landward boundary. Lines 119 and 120 are located above a basement high, and the siliciclastic turbidite sequence is absent beneath the trench wedge. Along line 120, the package is only present seaward of the trench axis, and along line 119, there is a possible siliciclastic turbidite package beneath the accretionary prism. The siliciclastic turbidite unit is also absent in lines 129–134 (Fig. 4), which have a smooth basement with gradual changes in basement depth.

The overlying hemipelagic mudstone and pyroclastic/hemipelagic Shikoku Basin units both occur throughout the entire study area. The boundary between the hemipelagic and the pyroclastic/hemipelagic units has been debated following drilling in the Kumano transect (Underwood and Pickering, 2018), and the more recent definitions place the top unit boundary at the first occurrence of ash in the cores, which is difficult to interpret seismically. Therefore, we considered the hemipelagic and pyroclastic/hemipelagic sediment as one unit (pyroclastic/hemipelagic–hemipelagic) that has a downward decrease in ash layers.

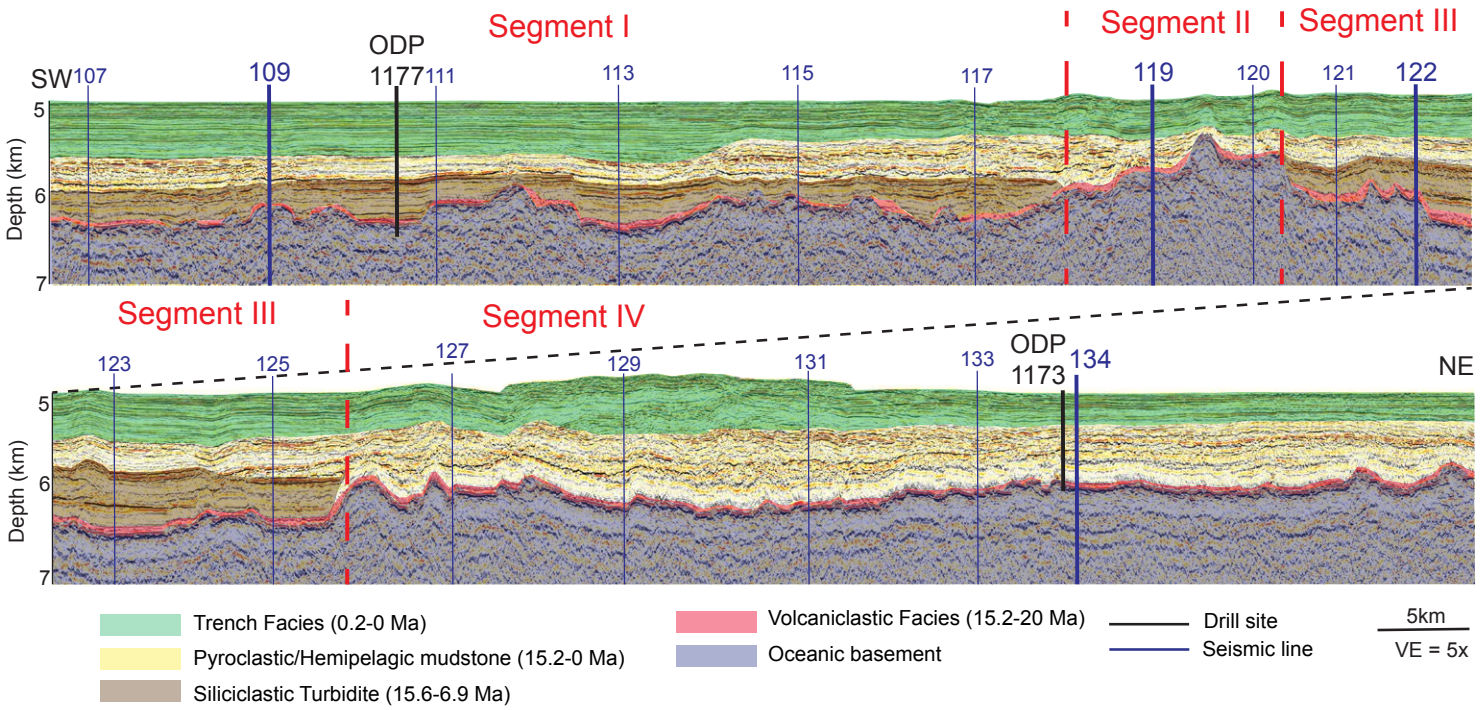

Figure 4. Seismic line KR9904–1 parallel to the trench (see Fig. 3 for exact location). Blue lines show the intersections of the seismic lines in Figures 7–10. Red dashed lines show segment boundaries. Black lines show projected locations of Ocean Drilling Program (ODP)/Deep Sea Drilling Project (DSDP) drill sites. Facies ages are from Underwood and Pickering (2018). VE—vertical exaggeration.

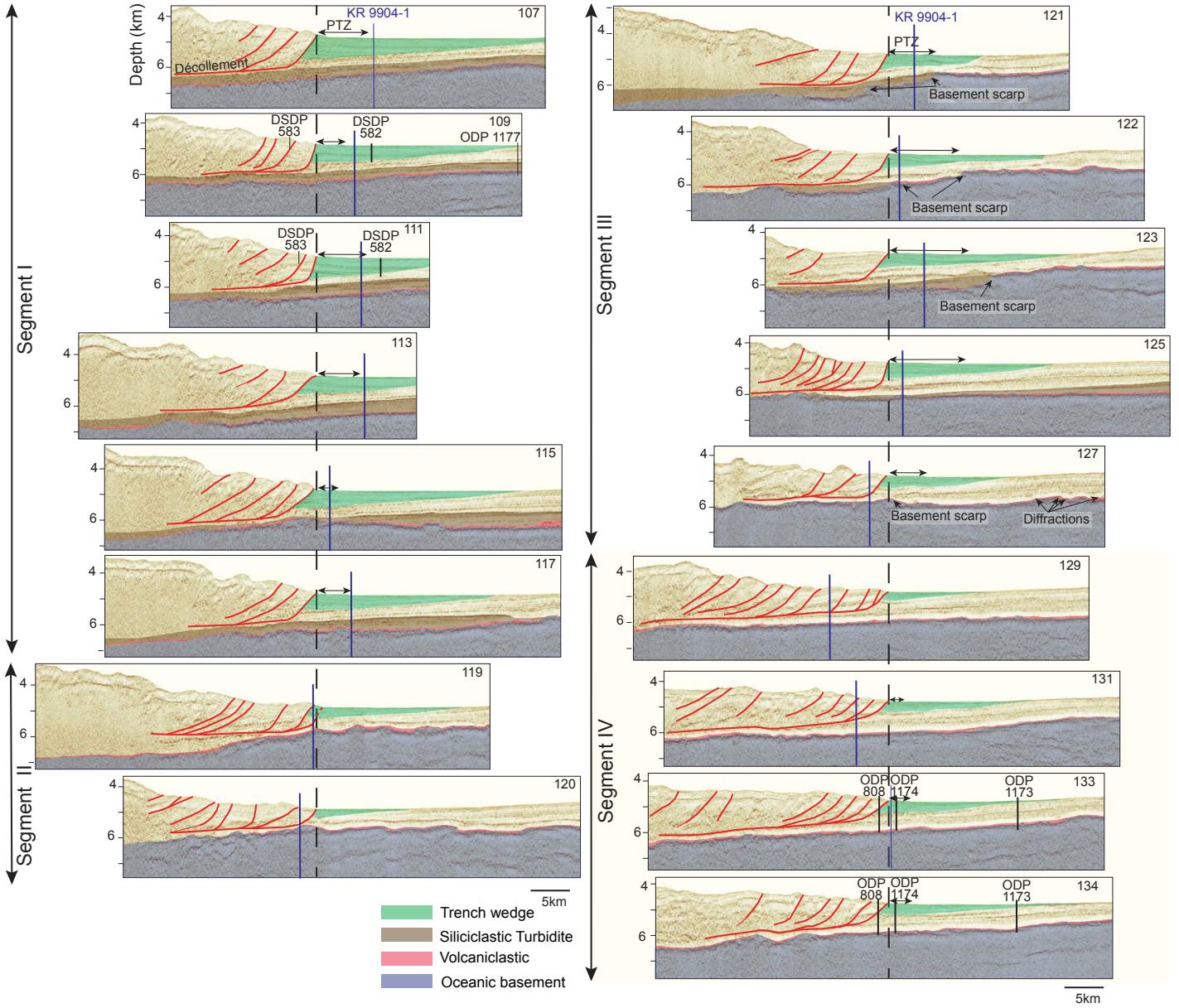

Figure 5. Depth-converted seismic reflection profiles of all the survey lines aligned by their frontal thrust. For line locations, see Figure 3. The protothrust zone (PTZ) extends seaward of the frontal thrust in most of the lines, and the protothrust zone width is highlighted by a black arrow. Where there is no black arrow, there is no clear protothrust zone. Red lines indicate the imbricate thrust faults and décollement. Blue lines are intersection with crossline KR9904-1. Black lines show projected locations of Ocean Drilling Program (ODP)/Deep Sea Drilling Project (DSDP) drill sites on the two lines on either side of each drill transect.

The pyroclastic/hemipelagic–hemipelagic Shikoku Basin sediments are buried beneath an upward-coarsening wedge of turbidites that forms the trench-fill unit. The trench-fill unit seaward of the frontal thrust makes up the trench wedge. The trench wedge varies along strike in thickness, width, and bounding characteristics (Fig. 6). The trench wedge width is the horizontal distance between the seafloor expression of the frontal thrust and the point of trench-fill onlap onto the pyroclastic/hemipelagic–hemipelagic sequence at the seafloor. The trench wedge thickness is measured between the seafloor and the base of the trench fill at the frontal thrust. The trench wedge is wide (~10–20 km) and thick (550–890 m) in the west and center (lines 107–117 and 121–127; Table 1; Figs. 6, 7, and 8). In contrast, lines 119–120 and 129–134 have a narrow (~8–14 km), thin (270–480 m) trench wedge (Figs. 9 and 10). Individual strongly reflective turbidite packages within the trench wedge become thinner and less reflective to the west (Fig. 4; Underwood and Pickering, 2018). We traced four marker horizons in the trench wedge throughout the area to use for structural analysis, which is discussed below.

Seismic Structure

We define the frontal thrust as the furthest seaward accretionary thrust fault that offsets the seafloor and has >30 m offset in all the sediment packages above the décollement. Incipient frontal thrusts in some lines have >30 m

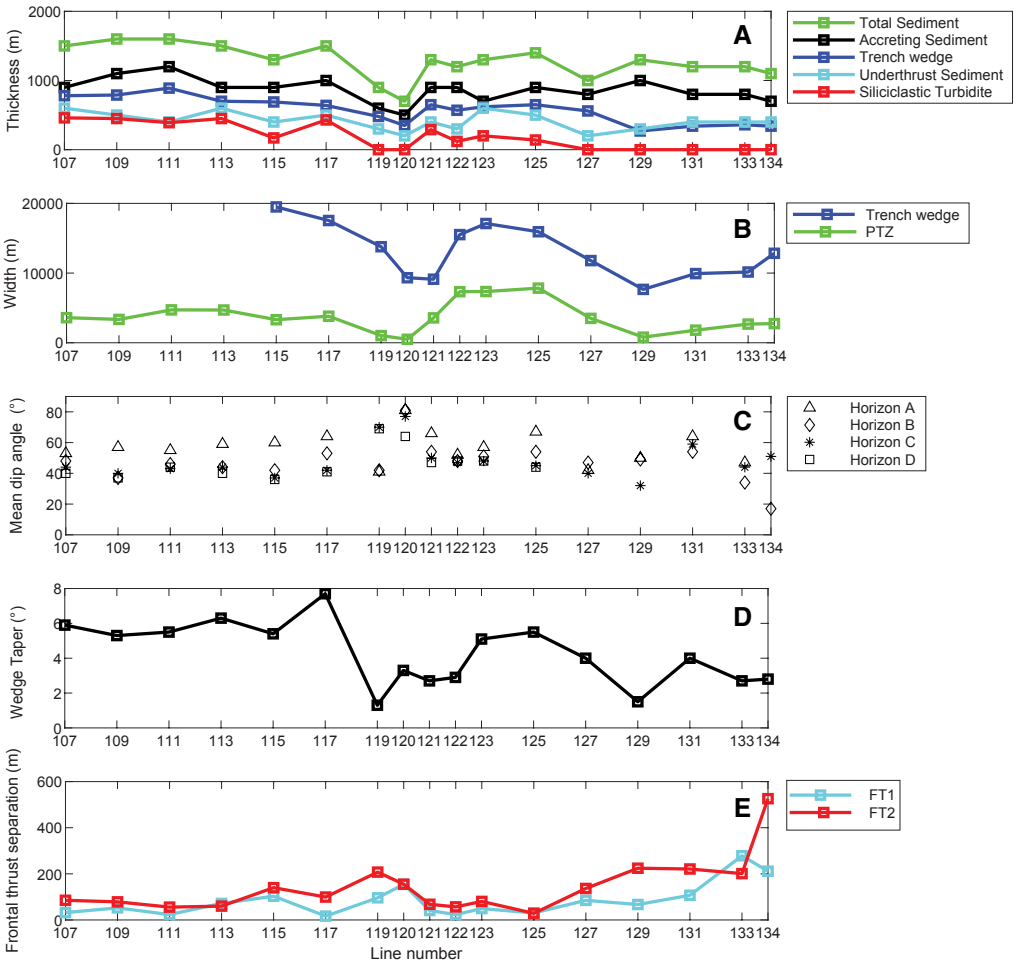

Figure 6. Plots of sediment and protothrust zone (PTZ) characteristics at each line. Each line is separated by 5 or 10 km along strike. (A) Sediment thickness measured at the frontal thrust. Accreting sediment is sediment above the décollement, and underthrust sediment is sediment beneath the décollement. (B) Plot of trench wedge and protothrust zone width at each line. The trench wedge width was measured between the frontal thrust and onlap of trench sediment onto the hemipelagic sediment. There are no data points for lines 107–113 because the seismic lines do not extend to the seaward edge of the trench wedge. Protothrust zone width is between the frontal thrust and deformation front. (C) Protothrust dip angle at each horizon. Not all horizons exist at every line. (D) Wedge taper of seaward three imbricated thrusts. (E) Mean separation of the first and second frontal thrusts (FT1 and FT2, respectively). The second frontal thrust was used to put the magnitude of the first frontal thrust in perspective, as in some lines FT1 is clearly incipient and still growing.

TABLE 1. STRUCTURAL MEASUREMENTS OF THE NANKAI TROUGH PROTOTHRUST ZONE

Segment	Line number	Maximum trench wedge thickness (m)	Maximum trench wedge width (m)	Siliciclastic turbidite thickness at deformation front (m)	Number of prototthrusts	Mean prototthrust dip at horizon (°)				Mean downdip extent (m)	Mean prototthrust spacing (m)	Mean polygonal fault dip (°)	Mean accreted prototthrust dip (°)
						Horizon A	Horizon B	Horizon C	Horizon D				
I	107	780	>20,780	460	108	53	48	44	40	444	34	71	55
	109	790	>19,910	450	70	57	37	40	37	424	49	79	54
	111	890	>10,950	390	92	55	46	43	44	596	52	69	54
	113	700	>9640	450	86	59	44	44	40	456	55	72	55
	115	690	19,490	170	54	60	42	37	36	399	62	74	69
	117	640	17,540	430	77	64	53	42	41	363	50	77	46
II	119	480	13,780	0	12	41	42	70	69	277	94	77	49
	120	350	9330	0	9	81	81	77	64	146	63	73	55
III	121	650	9120	290	60	66	54	50	47	324	61	77	56
	122	570	15,520	120	79	52	48	47	48	363	93	73	56
	123	620	17,110	200	82	57	51	48	48	346	89	76	46
	125	650	15,930	140	61	67	54	45	44	385	131	71	54
	127	560	11,790	0	47	42	47	40		327	76	71	60
IV	129	270	7660	0	10	50	49	32		176	89	78	53
	131	340	9925	0	15	64	54	59		284	129	77	67
	133	360	10,150	0	17	47	34	44		293	168	72	56
	134	340	12,840	0	17		17	51		343	172	75	64

offset in parts of the sediment, but they have not fully propagated from the décollement to the seafloor (Fig. 10).

The prototthrust zone is defined as the zone between the frontal thrust and the deformation front (Karig, 1986). Steep discontinuities with reverse-sense displacement within the prototthrust zone that strike subparallel to the frontal thrust are interpreted as prototthrusts. Polygonal normal faults in the Shikoku Basin sediment (Fig. 10; Heffernan et al., 2004) reduce the continuity of horizons, making it difficult to identify prototthrusts in the Shikoku Basin facies. The polygonal faults in the incoming Shikoku Basin facies occur across the entire region and become slightly degraded by compaction and deformation of sediment beneath the trench wedge. The faults have a mean dip of 74°, and there are an equal number of landward- and seaward-dipping faults in our 2-D seismic lines. The complexity and regional extent of these faults are the subject of work in progress and are beyond the scope of this paper. However, the polygonal normal faults do not appear to have a spatial relationship with the prototthrusts that would suggest they significantly influence the prototthrust zone characteristics.

The prototthrust zone width ranges from 0.5 to 7.8 km. Along-strike variations in the prototthrust zone width exist between four distinct segments (I–IV; Fig. 5). A relatively wide prototthrust zone exists between lines 107–117 (segment I) and 121–127 (segment III). Segments I and III have similar trench wedge widths but have different prototthrust zone widths (Table 1; Fig. 6). In segment I, there is a moderate-sized, 3–5-km-wide prototthrust zone, and there is a gradual transition from the prototthrust zone into a largely undeformed trench wedge (Fig. 7). In segment III, which contains the widest section of the prototthrust zone (3.5–8 km), the deformation front occurs furthest seaward, above a basement scarp (Fig. 8). Lines 119–120 (segment II) and 129–134 (segment IV) have narrow prototthrust zones (0.5–3 km) with relatively few prototthrusts (Figs. 9 and 10). The few (<20 per line) prototthrusts in these lines occur preferentially in the deepest part of the trench sediment near the toe of the frontal thrust.

STRUCTURAL ANALYSIS

Following Barnes et al. (2018), we measured the prototthrust dip, downdip extent, separation, and spacing (Fig. 11). We traced four trench wedge horizons (A–D) along strike to compare variations in deformation along strike and with depth (Figs. 7–10). A key horizon was chosen out of the interpreted horizons (A–D) for each line. The key horizon was the one that was intersected by most of the prototthrusts, and it was used to measure the spacing of the prototthrusts and the distance seaward of the frontal thrust. In lines 107–109, 115–127, and 134, it was horizon C, and in lines 111–113 and 129–133, it was horizon D.

Prototthrust Dip

The dip of every interpreted prototthrust was recorded at each of the four horizons to quantify variations in dip with depth (Fig. 6). The prototthrusts strike northeasterly, subparallel to the deformation front, and have predominantly

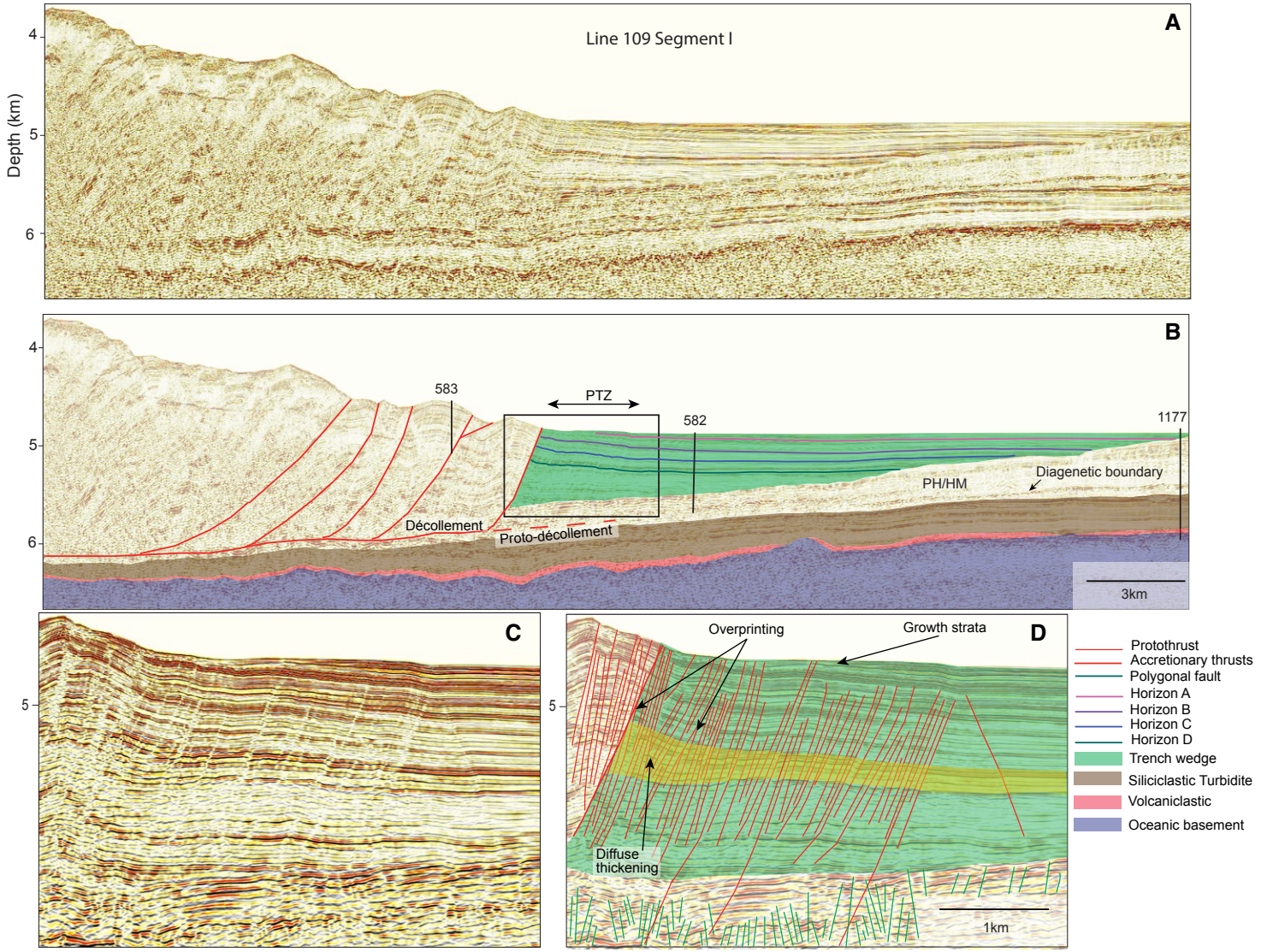

Figure 7. Depth-converted seismic reflection profile across the toe of the Nankai accretionary prism along line 109 in segment I. Location of the profile is shown in Figure 3. (A) Uninterpreted line 109 in segment I; vertical exaggeration (VE) = 3×. (B) Interpreted line 109 using stratigraphy defined at Ocean Drilling Program (ODP)/Deep Sea Drilling Project (DSDP) drill sites (see Fig. 2). Sites 583 and 1177 were projected onto the line perpendicular to the local structural trend. Black rectangle is the area enlarged in C–D. (C) Uninterpreted enlargement of A. (D) Interpreted enlargement of B. Yellow color highlights a sediment package that has undergone vertical extension and diffuse thickening. PTZ—protothrust zone; PH/HM—pyroclastic/hemipelagic–hemipelagic mudstone.

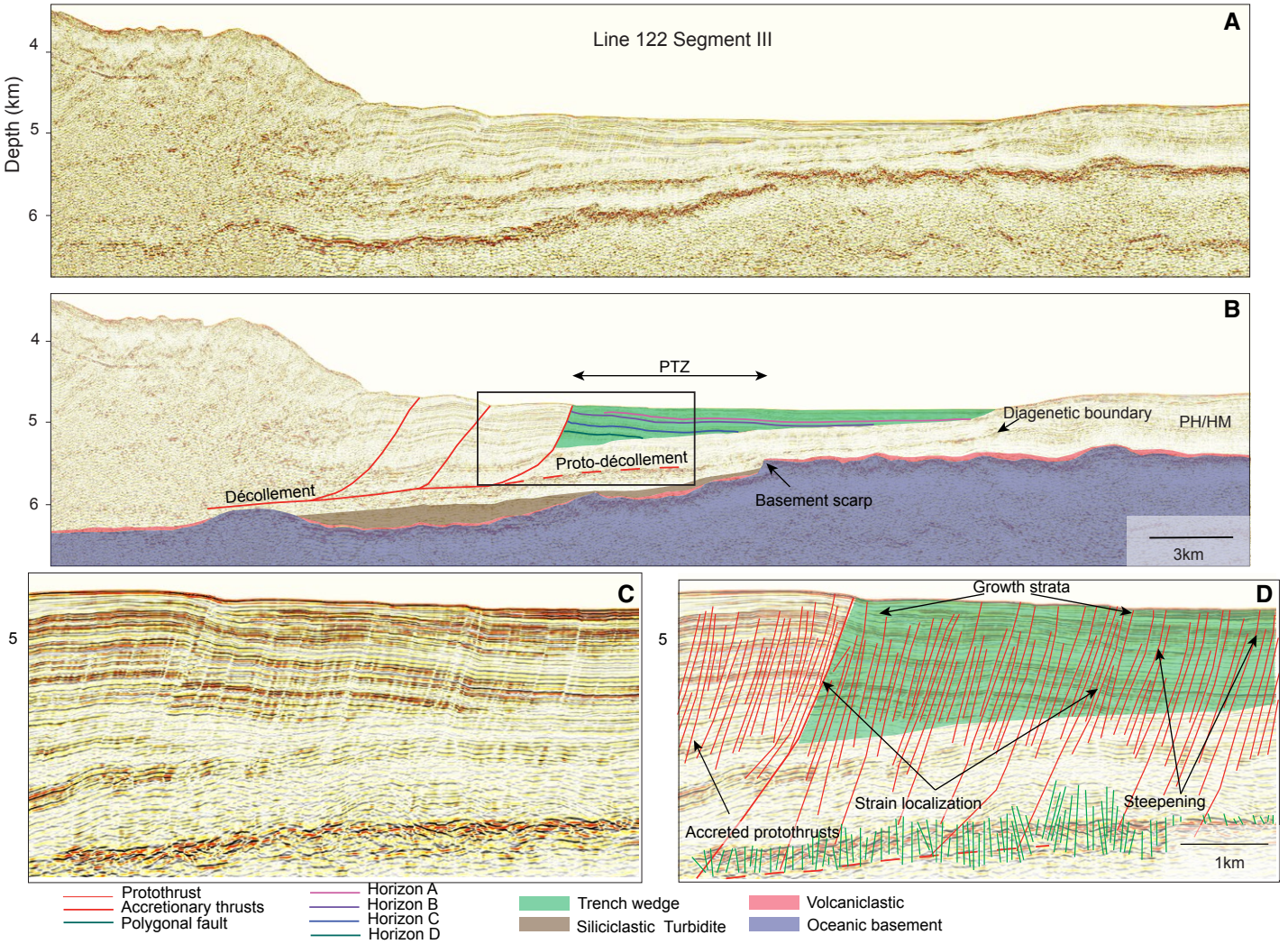

Figure 8. Depth-converted seismic reflection profile across the toe of the Nankai accretionary prism along line 122 in segment III. Location of the profile is shown in Figure 3. (A) Uninterpreted line 122, vertical exaggeration (VE) = 3×. (B) Interpreted line 122 using stratigraphy defined at Ocean Drilling Program (ODP) drill sites (see Fig. 2). Black rectangle is the area enlarged in C–D. (C) Uninterpreted enlargement of A. (D) Interpreted enlargement of B. PTZ—protothrust zone; PH/HM—pyroclastic/hemipelagic–hemipelagic mudstone.

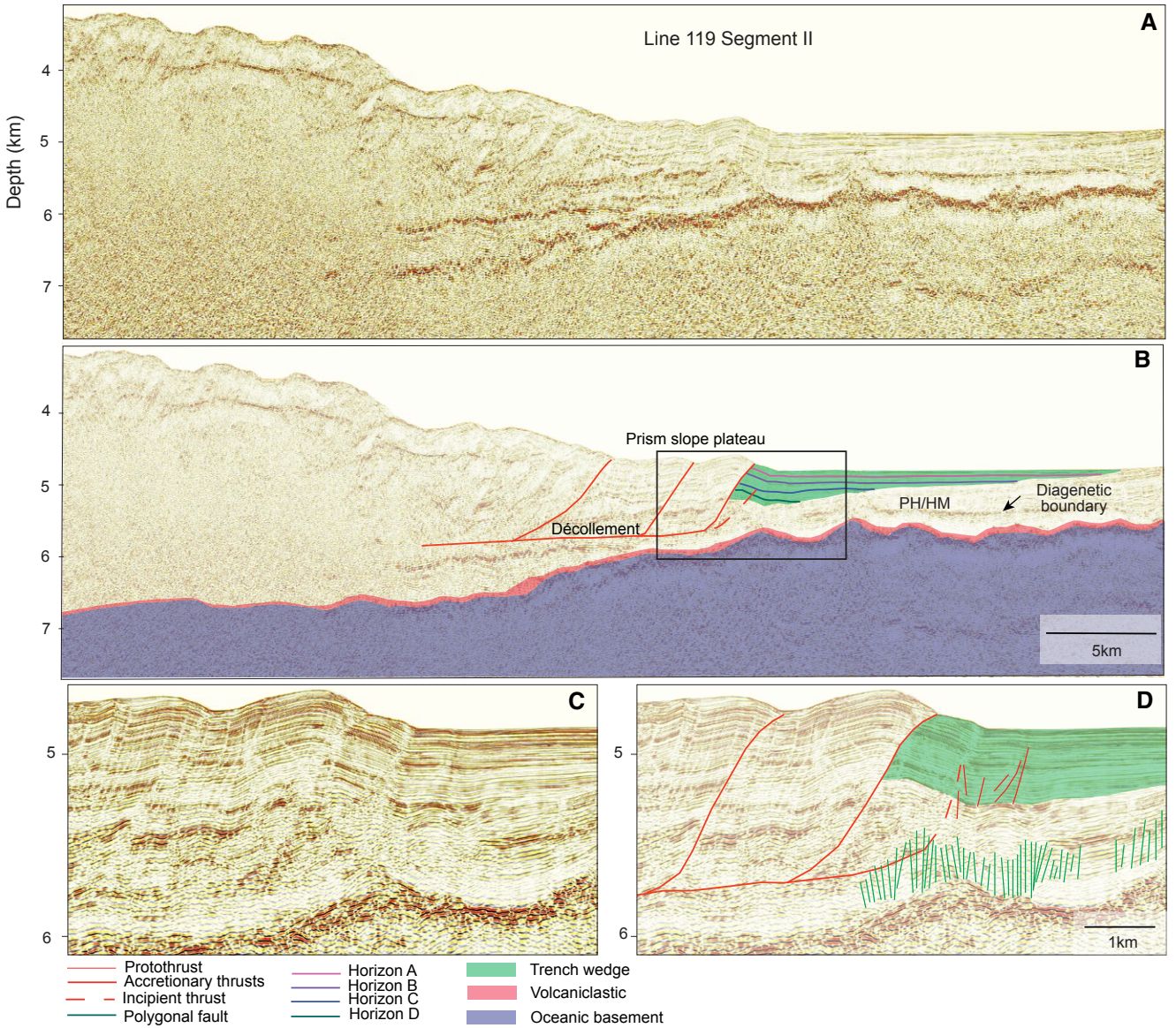

Figure 9. Depth-converted seismic reflection profile across the toe of the Nankai accretionary prism along line 119 in segment II. Location of the profile is shown in Figure 3. (A) Uninterpreted line 119, vertical exaggeration (VE) = 3×. (B) Interpreted line 119 using stratigraphy defined at Ocean Drilling Program (ODP) drill cores (see Fig. 2). There is a possible siliciclastic turbidite package beneath the accretionary prism, but the seismic characteristics of this package are unclear because of the signal attenuation of the more consolidated accretionary prism. Black rectangle is the area enlarged in C–D. (C) Uninterpreted enlargement of A. (D) Interpreted enlargement of B. PH/HM—pyroclastic/hemipelagic–hemipelagic mudstone.

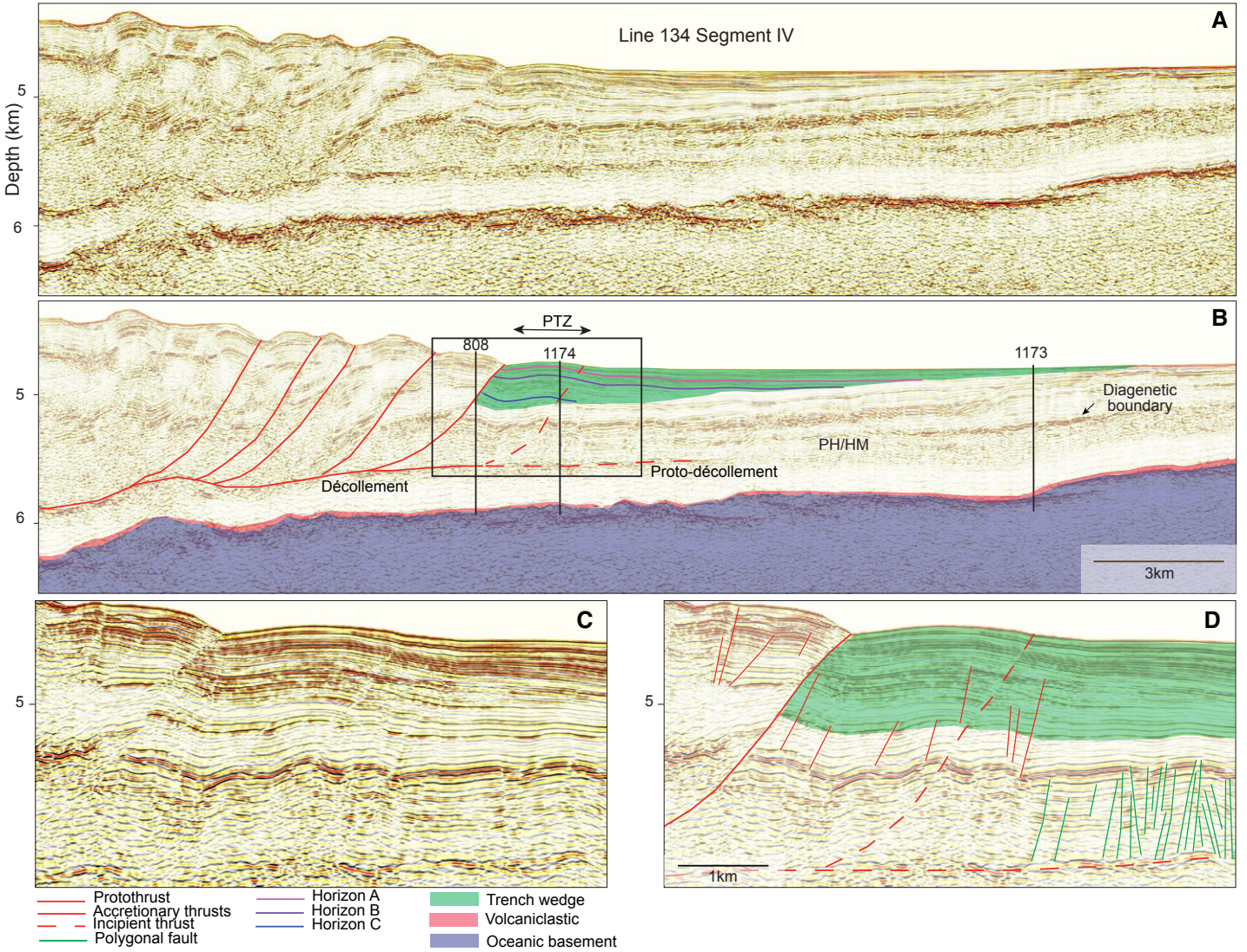

Figure 10. Depth-migrated seismic reflection profile across the toe of the Nankai accretionary prism along line 134 in segment IV. Location of the profile is shown in Figure 3. (A) Uninterpreted line 134, vertical exaggeration (VE) = 3×. (B) Interpreted line 134 using stratigraphy defined at Ocean Drilling Program (ODP) drill sites (see Fig. 2). ODP Sites 808, 1173, and 1174 are projected onto the line perpendicular to the local structural trend. Black rectangle is the area enlarged in C–D. (C) Uninterpreted enlargement of A. (D) Interpreted enlargement of B. PTZ—protothrust zone; PH/HM—pyroclastic/hemipelagic–hemipelagic mudstone.

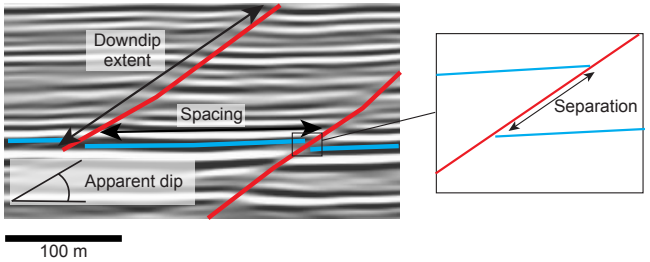

Figure 11. Prototthrust in a seismic profile showing the apparent fault dip, downdip extent, spacing, and separation (apparent relative displacement) measured. The total displacement (slip) of the fault cannot be measured because the direction of the fault displacement vector is not known. No vertical exaggeration in seismic section.

northwest dips. The protothrusts steepen upward and show distinct changes in dip at some shallow, strongly reflective packages (Fig. 8). These packages correspond to the thick, sandy turbidites identified in ODP cores (Moore et al., 2001). The mean dips of the individual protothrusts in segment I range from 37° to 64°; however, all of the steepest dips are recorded at horizon A. The mean dip is 37° to 53° if horizon A is excluded. The mean protothrust dips in segment III are 40° to 67° (40°–54° excluding horizon A), which is similar to protothrust dips in segment I and is consistent with high-angle, compactive shear bands associated with porosity reduction recorded in ODP drill cores (Karig and Lundberg, 1990; Ujiie et al., 2004). These dip angles are higher than predicted for Coulomb shear, which is ~30° to the subhorizontal maximum compressional stress (Morgan et al., 2007). The dips of the protothrusts in segments II and IV have more variability than those in segments I and III (Fig. 6). Segment II has mean dips of 41°–81°, and segment IV has mean dips of 17°–64°. The variability of the dips in narrow protothrust zones may be the result of the fractures forming due to bending stresses associated with fault-bend fold propagation (Fig. 10D) rather than the same mechanism that produced the approximately parallel protothrusts in segments I and III.

Protothrusts also occur in the hanging walls of the frontal thrusts (Figs. 7 and 8). These protothrusts correlate with the deformation bands in drill cores at DSDP Site 583, which dip between 25° and 60° (Karig and Lundberg, 1990). The accreted protothrusts were measured at approximately the same stratigraphic horizon as horizon C. The mean dip of the accreted protothrusts is 54°, which is higher than the mean protothrust dip at horizon C within the protothrust zone (48°; Table 1).

Protothrust Spacing

The spacing between protothrusts was measured as the horizontal distance between two protothrusts along the key horizon. The mean protothrust spacing increases with the protothrust zone width but shows a different trend for wide (segments I and III) versus narrow (segment II and IV) protothrust zones (Fig. 12). This difference supports our interpretation that the mechanisms that produce protothrusts at wide and narrow protothrust zones are different.

The spacing within each protothrust zone predominantly decreases landward (Fig. 13), which is consistent with an increase in strain. Interestingly, the landward reduction in protothrust spacing is not linear; clusters of closely spaced protothrusts occur in the areas that are associated with seafloor deformation and lower-angle protothrusts (e.g., Figs. 8 and 13). These locations are interpreted as the locations of incipient frontal thrusts.

Protothrust Downdip Extent

The downdip extent was recorded as the distance between the upper and lower tips of the fault (Fig. 11). Protothrust downdip extents are likely to be minimum values because the resolution decreases from ~3 m in the shallow sediment to ~15 m in the deepest sediment, so the deepest part of the protothrusts may be below the resolution of the seismic image. Additionally, the protothrusts were more clearly imaged in sediment with strong reflectivity. Therefore, lithological variations may result in a variable ability to image protothrusts, especially within the Shikoku Basin sediment. Protothrusts were difficult to interpret in the Shikoku Basin facies in the eastern protothrust zone because

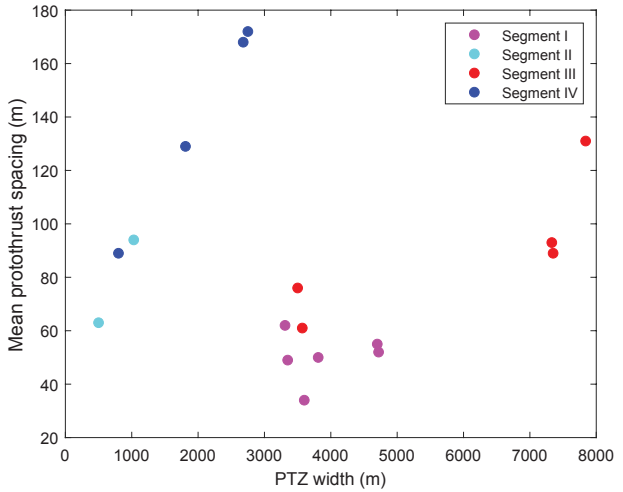

Figure 12. Plot of mean protothrust spacing against protothrust zone (PTZ) width. There are two main clusters: Blue circles represent the segments without a wide protothrust zone, and pink and red circles represent the segments with a wide protothrust zone. Both clusters show an increase in mean protothrust zone spacing with protothrust zone width.

it is acoustically weak. Furthermore, the presence of polygonal normal faults within the subducting sediment made it hard to discern overprinted protothrusts. The range of protothrust downdip extents is similar at both the western and eastern wide sections of the protothrust zone (segments I and III), but the mean is less at the protothrust zone in segment III as compared to segment I (Table 1). This is despite a similar maximum trench wedge thickness in both segments. In both segments, some protothrusts penetrate from the décollement to the seafloor, but most protothrusts are confined to the trench wedge (e.g., Fig. 7). The thickness, extent, and lithology of the Shikoku Basin facies vary locally (Ike et al., 2008), which might cause differences in the likelihood of protothrusts penetrating beneath the trench fill, or the degree to which protothrusts are imaged. The protothrusts that penetrate deeper tend to have a shallower dip at depth (Table 1), and changes in dip commonly occur at strongly reflective horizons, which may represent a change in lithology or sediment properties (e.g., Fig. 8).

DISCUSSION

Factors Controlling Protothrust Zone Size and Characteristics

Basement Topography

The protothrust zone width is clearly influenced by the subducting basement topography. The wide protothrust zone in segment I is above the smoothest portion of the oceanic crust, whereas the protothrust zone narrows significantly in segment II, where there is a subducting seamount (line 119–120). Additionally, the wide protothrust zone in segment III is above a smooth portion of the oceanic crust and terminates at the deformation front above the location of a basement scarp (Fig. 8). The relationship between the deformation front and basement scarps in segments III and IV is shown in Figure 14. In segment III, the basement topography influences the location of an area of high strain identified by greater protothrust displacement and associated seafloor uplift (Fig. 8), which is the probable location of a future frontal thrust. Previous studies show that steps in basement topography can effectively pin the deformation front to a particular location (Thomas, 1977; Bahroudi and Koyi, 2003; Vidal-Royo et al., 2009). Therefore, the basement scarp may explain why the protothrust zone is wider in segment III than in segment I despite a similar trench wedge width.

Basement topography also influences the thickness of sediment cover (Fig. 14), which is discussed in the following sections. Models show that the deformation front propagates further seaward of the frontal thrust where the sediment cover is thicker (e.g., Marshak et al., 1992). Therefore, where basement topography causes a sudden lateral change in the sediment thickness, the deformation front may bend along strike as a result of differential propagation of deformation (Farzipour-Saein et al., 2013). As a result, steps in the basement topography may explain the abrupt changes in deformation front location and thus the width of the protothrust zone in our survey area.

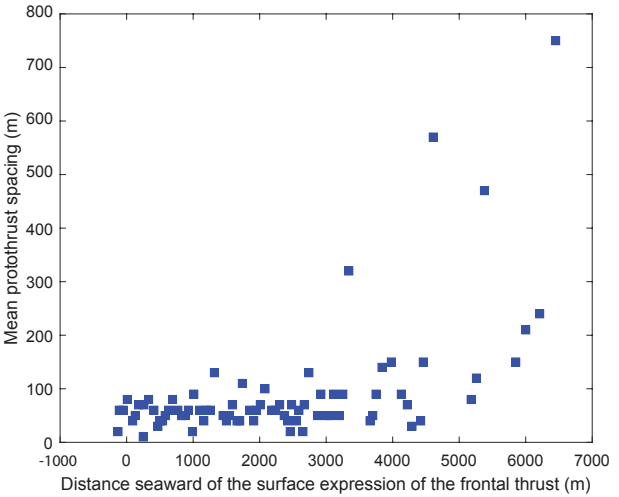

Figure 13. Plot of the spacing between protothrusts against the horizontal distance of the protothrust along horizon C from the seaward expression of the deformation front at line 122. The separation increases with distance from the frontal thrust, and there are a few clusters of closely separated protothrusts (Fig. 8).

Subducting Sediment Section

The seismic lines with a relatively narrow protothrust zone at the Nankai Trough are the same lines in which the siliciclastic turbidite unit is absent from the subducting hemipelagic facies (Fig. 6). The only exception is line 127, which has a relatively wide protothrust zone but does not have a siliciclastic turbidite unit. However, diffraction noise above the oceanic basement (Fig. 5) may be the result of this line on the very edge of a basement feature and could mark the transition between areas with and without the siliciclastic turbidite unit. The protothrusts do not penetrate the siliciclastic turbidite unit, so if the siliciclastic turbidite sediment controls protothrust formation, its influence must be indirect, such as by modifying the local stress state. At the Nankai Trough, lithologic variability (the presence of siliciclastic turbidite) is the primary factor controlling the décollement pore pressure (Saffer and Bekins, 2002). High pore pressures are common because the low-permeability hemipelagic sediment cap prevents pore-fluid escape at a rate comparable to the loading during sedimentation and subduction (Moore et al., 2001; Gamage and Screaton, 2006). However, the siliciclastic turbidite facies is more permeable than the hemipelagic/pyroclastic–hemipelagic facies, and the siliciclastic turbidite allows fluid to be expelled as it is compressed, reducing the pore pressure along the décollement (Karig and Morgan, 1994; Underwood and Pickering, 2018). The inferred décollement pore-pressure variations are consistent with

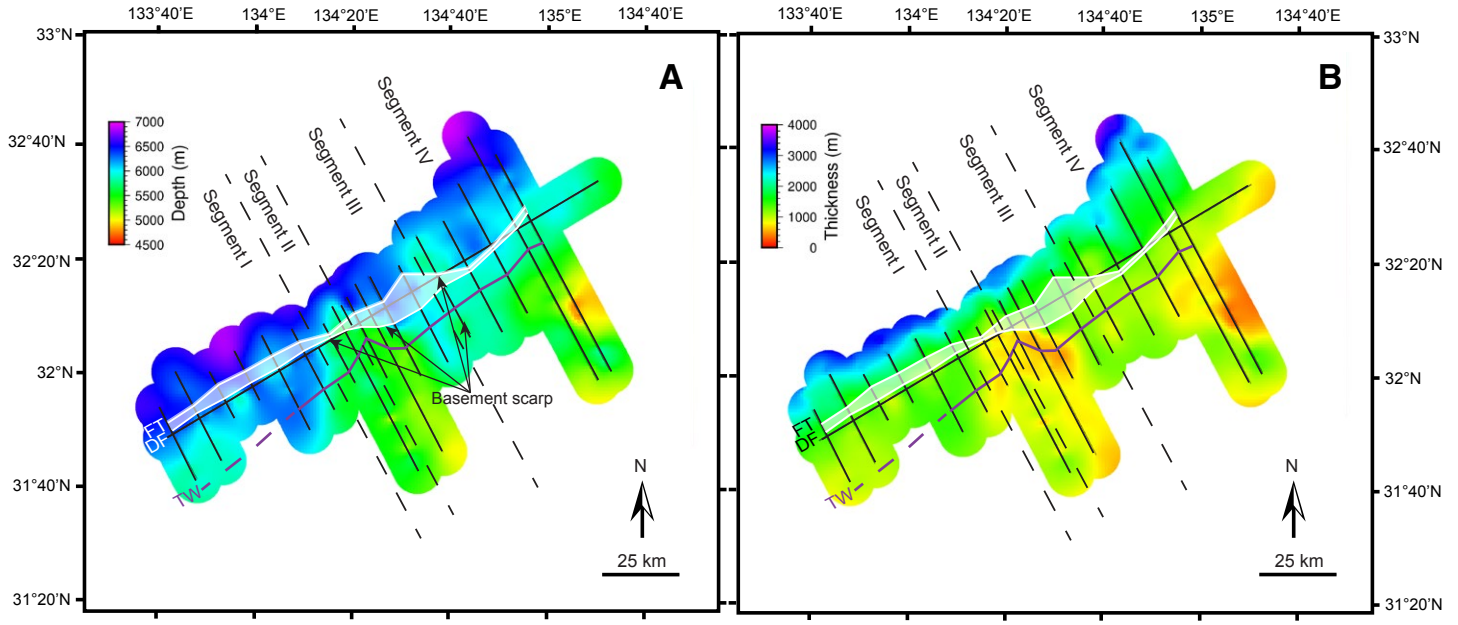

Figure 14. Gridded surface map of (A) top of the basement and (B) sediment thickness. FT—frontal thrust, DF—deformation front, TW—trench wedge.

the differences in wedge taper measured along the Ashizuri and Muroto transects (Moore et al., 1990), which correspond to the western and eastern parts of our survey area, respectively. The differences in wedge taper are interpreted to reflect a high basal strength along the Ashizuri transect due to better drainage along the décollement (Saffer, 2010). In our data, we see that changes in the prism geometry are consistent with changes in the subducting lithology and basement topography (Fig. 6).

Simple analytical models have been used to explain the influence of décollement pore pressure on deformation in the trench wedge (Wang et al., 1994; Weiss et al., 2018). Wang et al. (1994) hypothesized that an incipient décollement with high pore pressure is required seaward of the frontal thrust for stress to transfer to the footwall and a protothrust zone to form. Their model also showed that the magnitude of pore pressure within the incipient décollement may control the width of the protothrust zone. However, this model predicts that the protothrust zone would be wider in the eastern part of our study area, where the décollement pore pressure is higher and the wedge taper is lower than in the west, which is not the case. Therefore, although the entire Nankai margin must have sufficiently high incipient décollement pore pressure to transmit stress a few kilometers seaward of the frontal thrust, the presence of the subducting siliciclastic turbidite package and its reduction in the décollement pore pressure cannot explain the differences in the maximum width of the wide protothrust zone in segments I and III because the relationship between the protothrust zone width and the presence of the siliciclastic turbidite unit is the opposite of what the Wang et al. (1994) model predicts (Fig. 6).

Trench Wedge

The Nankai protothrust zone is widest where there is a wide and thick trench wedge (Fig. 6; Table 1). This observation agrees with previous studies that show that deformation at accretionary margins can be influenced by the thickness and type of accreting sediment (e.g., Marques and Cobbold, 2002). The thickness of the trench wedge sediment may influence the consolidation rate and thus the mechanical behavior of the trench wedge sediment. For example, turbidite deposition within the trench wedge can drive loading and consolidation of sediment within and beneath the wedge (Hüpers et al., 2018). As a result, a wide, thick trench wedge is likely to have more consolidated trench-fill sediment seaward of the frontal thrust than a narrow, thin trench wedge.

The size of the Nankai Trough trench wedge is controlled by the terrigenous sedimentation rate, which in turn is controlled by the magnitude, frequency,

and pathways of turbidity current flows (Mountney and Westbrook, 1996). Along-strike variations in the sedimentation rate are largely due to the subducting fossil Shikoku Basin spreading center axis, which forms a bathymetric high (Underwood and Pickering, 2018). The easternmost lines (segment IV) are adjacent to the higher topography of the extinct spreading center, which limits the amount of sediment that reaches the site from the axial turbidity currents that travel from the northeast (Pickering et al., 1993). As a result, a narrower trench wedge of 7–13 km has existed over the last 0.5 m.y. (Mountney and Westbrook, 1996). In contrast, near the westernmost lines (segment I), the trench wedge has been much wider (13–21 km) over the last 1 m.y. Segment I is located above a closed basement low, which has been a site with high sedimentation rate due to sediments derived both along the axis from the Izu-Bonin collision zone, as well as from the proximal Ashizuri Canyon (Pickering et al., 1992). These sediments extend as far as segment III. However, segment II is located along a bathymetric high, which acted as a barrier to the turbidity currents. The turbidity currents were diverted around the highs in segment II before being deposited in the lows of segment I.

Although the segments with a wide trench wedge correlate with those that have wide protothrust zones, the width of the trench wedge does not correlate directly with the maximum width of wide protothrust zones (Fig. 6). For example, segments I and III have similar trench wedge widths but different protothrust zone widths. Lithological variations in the trench wedge are also likely to influence the protothrust characteristics. At the Nankai Trough, the protothrusts steepen upward at the base of the strongly reflective sandy turbidites, highlighting a lithological control over protothrust characteristics. Strongly reflective turbidite packages occur throughout the entire study area, but they become thinner and less reflective to the west. These packages correlate with sand and silt turbidites that are more abundant and thicker in the trench wedge at the Muroto transect drill sites (segment IV) than the Ashizuri transect drill sites (segment I), which has a greater proportion of hemipelagic mud (Moore et al., 2001). The gradual along-strike changes in the trench wedge lithology do not correlate with the distinct segments that have wide protothrust zones at the Nankai Trough, so they are likely not a primary control over the protothrust zone width. However, they may have a secondary control that could explain the difference in protothrust zone width between segments I and III.

Protothrust Formation

The high-resolution data in this study revealed many protothrusts that have displacements greater than the seismic resolution (~3 m), whereas deformation bands in cores mostly have displacements of <1 mm and thicknesses of 1 mm to 1 cm, which are below seismic resolution (Karig and Lundberg, 1990). This leads us to suggest that the protothrusts are fractures that may evolve from deformation bands.

Deformation bands can reduce the porosity of sediment by up to an order of magnitude, and once a rock becomes cohesive with reduced porosity, deformation tends to occur by fracture propagation. Patches of slip surfaces can form in deformation band clusters (Aydin and Johnson, 1978), which can connect and develop into a continuous slip surface or fault (Shipton and Cowie, 2003). The protothrusts appear to nucleate in the lower half of the trench wedge turbidites, where the sediment is more consolidated. This depth is where the protothrust offset and the frequency of protothrusts are greatest. The protothrusts then grow updip and downdip, which is consistent with protothrust growth models (Weiss et al., 2018) and a previous study at the Hikurangi margin (Barnes et al., 2018). Therefore, although deformation bands form in underconsolidated sediment in the seaward portion of the trench wedge, they only evolve into protothrusts when the strata hosting the bands have undergone sufficient consolidation.

The timing of consolidation within the trench wedge may be a key control over the formation of wide protothrust zones. If consolidation occurs too far from the frontal thrust, such as by gravitational stresses, by the time it is subjected to compressive tectonic stresses in the vicinity of the frontal thrust, it is too consolidated for deformation bands to form. Conversely, if consolidation within the trench wedge is delayed or insufficient as the sediment approaches the frontal thrust, then deformation bands will not form shear surfaces or evolve into protothrusts. Variations in consolidation rate and strain localization could be due to a number of factors discussed above, including the subducting lithology and basement topography and the trench wedge geometry and lithology. Previous studies have shown that sediment consolidation within the trench wedge increases gradually in both the vertical and horizontal directions where there is a wide trench wedge in western Nankai (Morgan et al., 1994). This is the location of a wide protothrust zone (segment I). Where the trench wedge is narrower in eastern Nankai (segment IV), lateral increases in consolidation only occur much closer to the frontal thrust (Morgan and Karig, 1995). The delayed, rapid increase in consolidation in narrow trench wedges is not conducive to significant protothrust formation. These studies agree with our hypothesis that the trench wedge size may influence the consolidation rate of the sediment and thus control the width of the protothrust zone at the Nankai Trough.

Mean protothrust spacing in wide, well-established protothrust zones is greater where the protothrust zone is wider (Fig. 12). However, the protothrust spacing at wide, well-established protothrust zones cannot be compared with the protothrust spacing at narrow or barely existent protothrust zones. This is because the protothrusts appear to be formed by fundamentally different mechanisms (Barnes et al., 2018). The relationship between protothrust spacing and the width of the protothrust zone could be explained by a self-similar growth model of protothrust zones. This would mean that the protothrust zone grows by a constant balance between the development of new protothrusts within the protothrust zone and the creation of new protothrusts seaward of the current deformation front. Analogous behavior occurs in deformation bands in high-porosity sandstones, which show a logarithmic decrease in deformation band frequency away from a fault core (Anders and Wiltschko, 1994; Schueller et al., 2013). The distribution of deformation bands remains

self-similar as the width of the fault zone increases with time. The relationship between protothrust spacing and protothrust zone width is different between areas with a wide and narrow protothrust zone. This implies that the growth of protothrust zones occurs in a fundamentally different way in narrow and wide protothrust zones, and it is not simply a continuum where narrow protothrust zones will evolve into wide protothrust zones.

Implications for Strain Localization and Frontal Thrust Propagation

Protothrust spacing generally decreases landward, which may be due to the increase in consolidation and strain in the vicinity of the frontal thrust. However, clusters of closely spaced protothrusts with relatively higher cumulative displacement introduce heterogeneities in the seaward reduction in protothrust spacing (Fig. 6). We hypothesize that these clusters reflect strain localization and create zones of weakness along which the frontal thrust may propagate. This strain localization is well displayed in Figure 8D, where a cluster of protothrusts and growth strata occur in a concentrated area above a subducting basement scarp. The growth strata and seafloor uplift are interpreted to represent an incipient thrust fault. Once strain becomes localized seaward of the current frontal thrust, the strain rate on the current frontal thrust decreases significantly (Adam et al., 2005), and the incipient thrust fault becomes the new frontal thrust.

Most of the accreted protothrusts are likely to be inactive protothrusts that have been rotated to a steeper dip as the horizons underwent folding. However, it is plausible that some protothrusts may form landward of the frontal thrust in areas where the frontal thrust is young and the sediment within the thrust fault block is still undergoing rapid consolidation.

Areas with a well-established protothrust zone often have frontal thrusts that are listric, fault-propagation folds, with relatively low fault displacement (e.g., Figs. 6 and 9; Suppe and Medwedeff, 1990). In areas that are not adjacent to a wide protothrust zone, greater deformation along the frontal thrust occurs (Fig. 6), which is often accompanied by fault-bend folds (Suppe 1983). Fault-bend folds can evolve from fault-propagation folds where the frontal thrust has accommodated a large amount of strain (Marshak et al., 2019). In segment IV, where there is no significant subducting basement topography and no wide protothrust zone, the first few thrusts are fault-bend folds with large seafloor topography (130–240 m; Figs. 5 and 10). Conversely, in segment I, a wide protothrust zone occurs adjacent to a frontal thrust slice that has little displacement (40–140 m) and is largely associated with a fault-propagation fold (Figs. 5 and 7). Additionally, in segment III, where the protothrust zone is widest, the topography of the frontal thrust does not exceed 70 m (Figs. 3, 5, and 8). One possible explanation for the relationship between protothrust zone width and strain accommodation of the frontal thrust is that zones of weakness within well-established protothrust zones may promote forward propagation of the frontal thrust at a lower strain rate than at frontal thrusts that are not associated with a wide protothrust zone. Where there is no wide protothrust zone, strain at the accretionary prism toe is accommodated by greater displacement along the frontal thrust and within the thrust slice. Alternatively, the steep dip of the protothrusts may promote deformation by fault-propagation folding. Hughes et al. (2014) showed that fault-bend folding is favored at low fault ramp dips, whereas fault-propagation folding is favored at high fault ramp dips. If the frontal thrust evolves from a cluster of high-angle protothrusts, then the initial dip of the frontal thrust is steeper than would be predicted for Coulomb shear, which is ~30° to the subhorizontal maximum compressional stress (Morgan et al., 2007).

We can infer temporal variations in accretionary processes along individual lines from the relationship between protothrust zone width and frontal prism geometry. The frontal 5–10 km of the accretionary prism in segment III has a very shallow slope (<3°), which is consistent with a wide protothrust zone. However, the prism steepens abruptly (6°–9°) above an increase in basement topography. The siliciclastic turbidite package is nonexistent or much thinner landward of the basement high. We determine that there was not a wide protothrust zone at the time the steeper portion of the wedge was accreting. Additionally, line 127 has the narrowest protothrust zone in segment III and appears to mark the present transition from narrow to wide protothrust zone. The sediment thickens seaward at the step in basement topography, which is directly beneath the frontal thrust (Fig. 5).

Abundant accreted protothrusts and a plateau in the prism slope in segment II may indicate that there was a wide protothrust zone prior to the recent subduction of a basement high (Fig. 9). There also appears to be a thick turbidite sequence (siliciclastic turbidite facies) beneath the accretionary prism, which onlaps the basement high. The coexistence of these characteristics further supports the suggestion that there is a relationship among sediment thickness, protothrust zone width, and frontal thrust geometry at the Nankai Trough subduction zone. Along line 121, the accretionary style may be transitioning from that with a wide to a narrow protothrust zone. The protothrust zone in line 121 is less than half as wide as the nearest line within segment III (Table 1), and the deformation front is pinned above the basement scarp. Seaward of the basement scarp, the sediment is considerably thinner, and there is no siliciclastic turbidite package. We predict that a fault-bend fold will form above the basement scarp in the absence of a wide protothrust zone, and the frontal wedge taper will increase, similar to the present accretionary processes occurring along lines 119 and 120.

Comparison with Other Margins

The only other subduction zone where comparable structural analysis of protothrust zones has been applied is the central Hikurangi margin of New Zealand (Barnes et al., 2018). The central Hikurangi margin has a convergence rate and accretionary processes that are similar to those in our study area. The dip angles of the protothrusts are also similar to those at Nankai and are consistent with compactive shear deformation bands. Additionally, the frontal

thrust is a high-angle fault-propagation fold (Ghisetti et al., 2016; Barnes et al., 2018), which is consistent with those adjacent to a wide protothrust zone at Nankai. Barnes et al. (2018) also observed an increase in strain localization seaward of the frontal thrust and associated reduction of strain rate on the current frontal thrust. However, significant differences exist between the two subduction zones. Protothrusts in Hikurangi initiate further seaward of the frontal thrust than at the Nankai Trough (25 km at Hikurangi vs. <8 km at Nankai). The difference in protothrust zone width can be explained by the thickness of the trench wedge siliciclastic sequence. In central Hikurangi, the trench wedge is 2.2–2.5 km (>4 km total sediment), which is 2–3 times the thickness at Nankai. At Hikurangi, the protothrusts initiate within and are largely confined to the turbidite sequence, which implies that rheology-related differences due to lithology and/or consolidation state vary with depth (Barnes et al., 2018). The lithology beneath the turbidite sequence is not conducive to protothrust formation and limits the downdip extent of the protothrusts. Lithological differences between the Nankai Trough and Hikurangi margin may explain the differences between the two protothrust zones.

Differences in trench wedge lithologies may explain why some accretionary margins that have thick incoming sediment sections do not have protothrust zones. At the Barbados margin, the youngest sediment is calcareous ooze and mud (Moore et al., 1982), and there is no wedge of sandy trench turbidites and thus no protothrust zone. However, at the Makran accretionary margin and southern Hikurangi margin, the incoming sediment is exceptionally thick (7 km and 9 km, respectively) and consists of sandy turbidites (Kopp et al., 2000; Plaza-Faverola et al., 2012), but there is no protothrust zone. The thick sandy wedges are highly permeable and lose most of their fluid during normal compaction prior to accretion. As a result, the sediment is well consolidated when it approaches the deformation front (Fruehn et al., 1997), which inhibits the formation of protothrusts.

The relationship between protothrusts and consolidation is exemplified at the Cascadia and Chile margins (Cochrane et al., 1994; Han et al., 2017; Olsen et al., 2020). At the Cascadia margin, along the Washington transect, where the sediment is overconsolidated from ~20 km seaward of the frontal thrust, there are no protothrusts. In contrast, along the Oregon transect, where a thick underconsolidated sediment sequence is being both subducted and accreted, the upper part of the sediment hosts protothrusts and becomes progressively consolidated (Han et al., 2017). The landward increase in velocity is more rapid in the protothrust zone than in the rest of the basin, which implies that consolidation is more rapid in the protothrust zone than in the rest of the basin (Cochrane et al., 1994). Along the Chile margin, protothrusts also only form in areas that have thick (~2.8 km) underconsolidated incoming sediment (Diaz, 1999; Olsen et al., 2020) and show greatest consolidation within the protothrust zone.

The sediment consolidation at Cascadia is related to the décollement depth. Where the décollement lies near (<0.6 km above) the basement, the entire incoming sediment section is subject to horizontal compression from the accretionary wedge, leading to overconsolidation. Where there is a thick section of subducted sediment (~1.4–1.7 km), the subducted sediment does not experience the horizontal compression from the wedge, and high porosity is maintained, resulting in a weak basal décollement (Han et al., 2017). A weak décollement results in less consolidation in the trench wedge (Davis et al., 1983), which is required for the formation of a protothrust zone (Wang et al., 1994). Consistent with the observations at Cascadia, the absence of a protothrust zone at the northern Hikurangi margin correlates with a thin (~500 m) layer of subducting sediment (Pedley et al., 2010) as well as a thin trench wedge, rough crust, and subducting seamounts (Barnes et al., 2020), similar to segment II.

Along most of the Sumatran margin, little sediment is subducted (McNeill et al., 2017), and the trench fill is more consolidated than many other subduction settings (Hüpers et al., 2017). As a result, there is no protothrust zone. However, variations in the depth of the décollement and the amount of sediment subducted are still shown to influence the frontal thrust propagation and fault vergence (Bradley et al., 2019).

A protothrust zone is largely absent along the Alaska-Aleutian margin. Along most of the margin, thin incoming sediment is the primary reason for no protothrust zone (Bécel et al., 2017). One exception is offshore the Kenai Peninsula, in the eastern portion of the margin, where there is sufficient sediment thickness to produce an ~12-km-wide protothrust zone, although less than five protothrusts were identified (von Huene et al., 1998). Seismic transects immediately to the northeast of that line do not have a protothrust zone despite having a wide and thick trench wedge and thick subducting sediment. These lines also have a narrow accretionary wedge and a steeper frontal wedge taper (Fruehn et al., 1999), which reflect the progressive evolution of the margin from erosion to accretion following the subduction of the Yakutat terrane (Fruehn et al., 1999). Recent tectonic erosion also occurred further west in the Semidi segment, where there is up to 3 km of trench fill and >900 m of subducted sediment but no protothrust zone (von Huene et al., 2012; Li et al., 2018). The recent subduction of major basement relief alters the local stress state, and there is commonly diminished lateral compression in the wake of subducted topography (Sun et al., 2020). Insufficient compressive stress in the trench wedge will inhibit the formation of a wide protothrust zone and/or significantly limit the number of protothrusts within the protothrust zone.

From the variations in protothrust formation between subduction margins, we conclude that thick trench wedge sediments must be underconsolidated and consist of sandy turbidites for protothrusts to form. We also find that consolidation increases more rapidly where protothrusts form. Furthermore, the margin must be in a well-established accretionary phase, as recent erosional phases appear to inhibit the formation of protothrust zones.

CONCLUSIONS

The protothrust zone at the toe of the Nankai Trough accretionary prism shows great along-strike variability. Two spatially discrete segments have a wide protothrust zone (~3.3–7.8 km, ~50–110 protothrusts), but these are

bounded by segments with almost no protothrust zone (~0.5–2.8 km, <20 protothrusts). At the Nankai Trough, the primary control over the presence of a wide protothrust zone seems to be the trench wedge size, which influences the progression of sediment consolidation. Secondary controls over the maximum width of wide protothrust zones include the accreting lithology and the subducting basement topography.

The majority of the Nankai protothrusts have a high dip angle, consistent with compactive shear bands in drill cores. We hypothesize that the protothrusts are fractures that form from shear surfaces in deformation band clusters that have undergone porosity reduction where the trench-fill sediment is more consolidated. Closely spaced protothrusts are associated with strain localization and may become the locations of frontal thrust propagation. Forward propagation of frontal thrusts as fault-propagating folds may occur at a lower buildup of strain than where mature protothrusts are absent. Where there is a narrow or no protothrust zone, there is greater displacement along the frontal thrust, which is probably due to greater strain buildup along the frontal thrust. Alternatively, the protothrusts may dictate the dip at which the frontal thrust forms and thus whether the frontal thrust is associated with a fault-bend or fault-propagating fold. Either way, it is clear that the protothrust zone influences deformation along the frontal thrust and thus the geometry of the accretionary prism.

ACKNOWLEDGMENTS

We thank the captain and crew of the R/V *Kaiyo* for assistance during seismic data acquisition, and we greatly appreciate the Japan Agency for Marine-Earth Science and Technology (JAMSTEC) for providing us with the seismic data. All seismic surveys were supported by the "Research Project for Compound Disaster Mitigation on the Great Earthquakes and Tsunamis around the Nankai Trough Region" of the Ministry of Education, Culture, Sports, Science and Technology (MEXT) of Japan. This paper was improved by the reviews of earlier drafts by Roland von Huene, Julia Morgan, Helen Janiszewski, and Garrett Ito. Special thanks go to Phil Barnes for his extremely thorough review and suggestions. We also thank Guest Associate Editor Dave Scholl for his timely handling of the manuscript. This work was supported by National Science Foundation grant OCE-1658580. This is University of Hawaii School of Ocean and Earth Science and Technology (SOEST) contribution 11176.

REFERENCES CITED

Adam, J., Urai, J., Wieneke, B., Oncken, O., Pfeiffer, K., Kukowski, N., Lohrmann, J., Hoth, S., Van Der Zee, W., and Schmatz, J., 2005, Shear localisation and strain distribution during tectonic faulting—New insights from granular-flow experiments and high-resolution optical image correlation techniques: Journal of Structural Geology, v. 27, no. 2, p. 283–301, https://doi.org/10.1016/j.jsg.2004.08.008.

Anders, M.H., and Wiltschko, D.V., 1994, Microfracturing, paleostress and the growth of faults: Journal of Structural Geology, v. 16, no. 6, p. 795–815, https://doi.org/10.1016/0191-8141(94)90146-5.

Aydin, A., and Johnson, A.M., 1978, Development of faults as zones of deformation bands and as slip surfaces in sandstone: Pure and Applied Geophysics, v. 116, no. 4–5, p. 931–942, https://doi.org/10.1007/BF00876547.

Bahroudi, A., and Koyi, H., 2003, Effect of spatial distribution of Hormuz Salt on deformation style in the Zagros fold and thrust belt: An analogue modelling approach: Journal of the Geological Society [London], v. 160, no. 5, p. 719–733, https://doi.org/10.1144/0016-764902-135.

Bangs, N.L., Shipley, T.H., Gulick, S.P., Moore, G.F., Kuromoto, S., and Nakamura, Y., 2004, Evolution of the Nankai Trough décollement from the trench into the seismogenic zone: Inferences from three-dimensional seismic reflection imaging: Geology, v. 32, no. 4, p. 273–276, https://doi.org/10.1130/G20211.2.

Barnes, P.M., Ghisetti, F.C., Ellis, S., and Morgan, J.K., 2018, The role of protothrusts in frontal accretion and accommodation of plate convergence, Hikurangi subduction margin, New Zealand: Geosphere, v. 14, no. 2, p. 440–468, https://doi.org/10.1130/GES01552.1.

Barnes, P.M., Wallace, L.M., Saffer, D.M., Bell, R.E., Underwood, M.B., Fagereng, A., Meneghini, F., Savage, H.M., Rabinowitz, H.S., and Morgan, J.K., 2020, Slow slip source characterized by lithological and geometric heterogeneity: Science Advances, v. 6, eaay3314, https://doi.org/10.1126/sciadv.aay3314.

Bécel, A., Shillington, D.J., Delescluse, M., Nedimović, M.R., Abers, G.A., Saffer, D.M., Webb, S.C., Keranen, K.M., Roche, P.-H., and Li, J., 2017, Tsunamigenic structures in a creeping section of the Alaska subduction zone: Nature Geoscience, v. 10, no. 8, p. 609, https://doi.org/10.1038/ngeo2990.

Bésuelle, P., 2001, Compacting and dilating shear bands in porous rock: Theoretical and experimental conditions: Journal of Geophysical Research: Solid Earth, v. 106, no. B7, p. 13435–13442, https://doi.org/10.1029/2001JB900011.

Bradley, K., Qin, Y., Carton, H., Hananto, N., Villanueva-Robles, F., Leclerc, F., Shengji, W., Tapponier, P., Sieh, K., and Singh, S., 2019, Stratigraphic control of frontal décollement level and structural vergence and implications for tsunamigenic earthquake hazard in Sumatra, Indonesia: Geochemistry Geophysics Geosystems, v. 20, no. 3, p. 1646–1664, https://doi.org/10.1029/2018GC008025.

Cochrane, G., Moore, J., MacKay, M., and Moore, G., 1994, Velocity and inferred porosity model of the Oregon accretionary prism from multichannel seismic reflection data: Implications on sediment dewatering and overpressure: Journal of Geophysical Research: Solid Earth, v. 99, p. 7033–7043, https://doi.org/10.1029/93JB03206.

Davis, D., Suppe, J., and Dahlen, F., 1983, Mechanics of fold-and-thrust belts and accretionary wedges: Journal of Geophysical Research: Solid Earth, v. 88, no. B2, p. 1153–1172, https://doi.org/10.1029/JB088iB02p01153.

Diaz, J., 1999, Sediment Subduction and Accretion at the Chilean Convergent Margin Between 35 and 40°S [Ph.D. dissertation]: Kiel, Germany, Christian-Albrechts-Universität zu Kiel, 253 p.

Farzipour-Saein, A., Nilfouroushan, F., and Koyi, H., 2013, The effect of basement step/topography on the geometry of the Zagros fold and thrust belt (SW Iran): An analog modeling approach: International Journal of Earth Sciences, v. 102, no. 8, p. 2117–2135, https://doi.org/10.1007/s00531-013-0921-5.

Fossen, H., Schultz, R.A., Shipton, Z.K., and Mair, K., 2007, Deformation bands in sandstone: A review: Journal of the Geological Society [London], v. 164, no. 4, p. 755–769, https://doi.org/10.1144/0016-76492006-036.

Fossen, H., Soliva, R., Ballas, G., Trzaskos, B., Cavalcante, C., and Schultz, R.A., 2018, A review of deformation bands in reservoir sandstones: Geometries, mechanisms and distribution, *in* Ashton, M., Dee, S.J., and Wennberg, O.P., eds., Subseismic-Scale Reservoir Deformation: Geological Society of London Special Publication 459, p. 9–33, https://doi.org/10.1144/SP459.4.

Fruehn, J., White, R., and Minshull, T., 1997, Internal deformation and compaction of the Makran accretionary wedge: Terra Nova, v. 9, no. 3, p. 101–104, https://doi.org/10.1046/j.1365-3121.1997.d01-13.x.

Fruehn, J., von Huene, R., and Fisher, M.A., 1999, Accretion in the wake of terrane collision: The Neogene accretionary wedge off Kenai Peninsula, Alaska: Tectonics, v. 18, no. 2, p. 263–277, https://doi.org/10.1029/1998TC900021.

Gamage, K., and Screaton, E., 2006, Characterization of excess pore pressures at the toe of the Nankai accretionary complex, Ocean Drilling Program Sites 1173, 1174, and 808: Results of one-dimensional modeling: Journal of Geophysical Research, v. 111, no. B4, B04103, https://doi.org/10.1029/2004JB003572.

Ghisetti, F.C., Barnes, P.M., Ellis, S., Plaza-Faverola, A.A., and Barker, D.H., 2016, The last 2 Myr of accretionary wedge construction in the central Hikurangi margin (North Island, New Zealand): Insights from structural modeling: Geochemistry Geophysics Geosystems, v. 17, p. 2661–2686, https://doi.org/10.1002/2016GC006341.

Guo, J., and Underwood, M.B., 2011, Data report: Refined method for calculating percentages of kaolinite and chlorite from X-ray diffraction data, with application to the Nankai margin of southwest Japan, *in* Kinoshita, M., et al., Proceedings of the Integrated Ocean Drilling Program, Volume 314/315/316: Washington, D.C., Integrated Ocean Drilling Program Management International, Inc., https://doi.org/10.2204/iodp.proc.314315316.201.2011.

Han, S., Bangs, N.L., Carbotte, S.M., Saffer, D.M., and Gibson, J.C., 2017, Links between sediment consolidation and Cascadia megathrust slip behaviour: Nature Geoscience, v. 10, no. 12, p. 954–959, https://doi.org/10.1038/s41561-017-0007-2.

Heffernan, A., Moore, J., Bangs, N., Moore, G., and Shipley, T., 2004, Initial deformation in a subduction thrust system: Polygonal normal faulting in the incoming sedimentary sequence of the Nankai subduction zone, southwestern Japan, *in* Davies, R.J., Cartwright, J.A., Stewart, S.A., Lappin, M., and Underhill, J.R., eds., 3D Seismic Technology: Application to the Exploration of Sedimentary Basins: Geological Society of London Memoir 29, p. 143–148, https://doi.org/10.1144/GSL.MEM.2004.029.01.14.

Hughes, A.N., Benesh, N.P., and Shaw, J.H., 2014, Factors that control the development of fault-bend versus fault-propagation folds: Insights from mechanical models based on the discrete element method (DEM): Journal of Structural Geology, v. 68, p. 121–141, https://doi.org/10.1016/j.jsg.2014.09.009.

Hüpers, A., Torres, M.E., Owari, S., McNeill, L.C., Dugan, B., Henstock, T.J., Milliken, K.L., Petronotis, K.E., Backman, J., and Bourlange, S., 2017, Release of mineral-bound water prior to subduction tied to shallow seismogenic slip off Sumatra: Science, v. 356, no. 6340, p. 841–844, https://doi.org/10.1126/science.aal3429.

Hüpers, A., Saffer, D., and Kopf, A., 2018, Lithostratigraphic controls on dewatering and fluid pressure in the western Nankai subduction zone: Implications for the drainage behavior and consolidation state of the underthrust sequence, *in* Byrne, T., et al., eds., Geology and Tectonics of Subduction Zones: A Tribute to Gaku Kimura: Geological Society of America Special Paper 534, p. 51–68, https://doi.org/10.1130/2018.2534(03).

Ike, T., Moore, G.F., Kuramoto, S.i., Park, J.-O., Kaneda, Y., and Taira, A., 2008, Variations in sediment thickness and type along the northern Philippine Sea plate at the Nankai Trough: The Island Arc, v. 17, no. 3, p. 342–357, https://doi.org/10.1111/j.1440-1738.2008.00624.x.

Ishii, T., 2000, Geological and petrological studies of the Kinan and Izu-Ogasawara backarc-echelon seamount chains: Bulletin of the Geological Survey of Japan, v. 51, p. 615–630.

Ishizuka, O., Yuasa, M., Taylor, R.N., and Sakamoto, I., 2009, Two contrasting magmatic types coexist after the cessation of back-arc spreading: Chemical Geology, v. 266, p. 274–296, https://doi.org/10.1016/j.chemgeo.2009.06.014.

Karig, D., 1986, The framework of deformation in the Nankai Trough, *in* Karig, D.E., and Kagami, H., et al., Initial Reports Deep Sea Drilling Projects, Volume 87: Washington, D.C., U.S. Government Printing Office, p. 927–940, https://doi.org/10.2973/dsdp.proc.87.138.1986.

Karig, D., and Lundberg, N., 1990, Deformation bands from the toe of the Nankai accretionary prism: Journal of Geophysical Research: Solid Earth, v. 95, p. 9099–9109, https://doi.org/10.1029/JB095iB06p09099.

Karig, D., and Morgan, J.K., 1994, Tectonic deformation: Stress paths and strain histories, *in* Maltman, A., ed., The Geological Deformation of Sediments: London, Chapman and Hall, p. 167–204, https://doi.org/10.1007/978-94-011-0731-0_6.

Kimura, G., Hashimoto, Y., Kitamura, Y., Yamaguchi, A., and Koge, H., 2014, Middle Miocene swift migration of the TTT triple junction and rapid crustal growth in southwest Japan: A review: Tectonics, v. 33, no. 7, p. 1219–1238, https://doi.org/10.1002/2014TC003531.

Kimura, G., Koge, H., and Tsuji, T., 2018, Punctuated growth of an accretionary prism and the onset of a seismogenic megathrust in the Nankai Trough: Progress in Earth and Planetary Science, v. 5, no. 1, p. 78, https://doi.org/10.1186/s40645-018-0234-1.

Kimura, J.-I., Stern, R.J., and Yoshida, T., 2005, Reinitiation of subduction and magmatic responses in SW Japan during Neogene time: Geological Society of America Bulletin, v. 117, no. 7–8, p. 969–986, https://doi.org/10.1130/B25565.1.

Kobayashi, K., and Nakada, M., 1978, Magnetic anomalies and tectonic evolution of the Shikoku inter-arc basin: Journal of Physics of the Earth, v. 26, Supplement, p. S391–S402.

Kobayashi, K., Kasuga, S., and Okino, K., 1995, Shikoku Basin and its margins, *in* Taylor, B., ed., Backarc Basins: Boston, Springer, p. 381–405, https://doi.org/10.1007/978-1-4615-1843-3_10.

Kopp, C., Fruehn, J., Flueh, E., Reichert, C., Kukowski, N., Bialas, J., and Klaeschen, D., 2000, Structure of the Makran subduction zone from wide-angle and reflection seismic data: Tectonophysics, v. 329, no. 1–4, p. 171–191, https://doi.org/10.1016/S0040-1951(00)00195-5.

Li, J., Shillington, D.J., Saffer, D.M., Bécel, A., Nedimović, M.R., Kuehn, H., Webb, S.C., Keranen, K.M., and Abers, G.A., 2018, Connections between subducted sediment, pore-fluid pressure, and earthquake behavior along the Alaska megathrust: Geology, v. 46, no. 4, p. 299–302, https://doi.org/10.1130/G39557.1.

Marques, F., and Cobbold, P., 2002, Topography as a major factor in the development of arcuate thrust belts: Insights from sandbox experiments: Tectonophysics, v. 348, no. 4, p. 247–268, https://doi.org/10.1016/S0040-1951(02)00077-X.

Marshak, S., Wilkerson, M., and Hsui, A., 1992, Generation of curved fold-thrust belts: Insight from simple physical and analytical models, *in* McClay, K.R., ed., Thrust Tectonics: Dordrecht, Netherlands, Springer, p. 83–92, https://doi.org/10.1007/978-94-011-3066-0_7.

Marshak, S., Haq, S.S., and Sen, P., 2019, Ramp initiation in fold-thrust belts: Insight from PIV analysis of sandbox models: Journal of Structural Geology, v. 118, p. 308–323, https://doi.org/10.1016/j.jsg.2018.11.006.

McNeill, L., Dugan, B., Petronotis, K., and the Expedition 362 Scientists, 2017, Sumatra Subduction Zone: Proceedings of the International Ocean Discovery Program, Volume 362: College Station, Texas, International Ocean Discovery Program, https://doi.org/10.14379/iodp.proc.362.2017.

Moore, G.F., Shipley, T., Stoffa, P., Karig, D., Taira, A., Kuramoto, S., Tokuyama, H., and Suyehiro, K., 1990, Structure of the Nankai Trough accretionary zone from multichannel seismic reflection data: Journal of Geophysical Research: Solid Earth, v. 95, no. B6, p. 8753–8765, https://doi.org/10.1029/JB095iB06p08753.

Moore, G.F., Taira, A., Klaus, A., Becker, L., Boeckel, B., Cragg, B.A., Dean, A., Fergusson, C.L., Henry, P., Hirano, S., Hisamitsu, T., Hunze, S., Kastner, M., Maltman, A.J., Morgan, J.K., Murakami, Y., Saffer, D.M., Sánchez-Gómez, M., Screaton, E.J., Smith, D.C., Spivack, A.J., Steurer, J., Tobin, H.J., Ujiie, K., Underwood, M.B., and Wilson, M., 2001, New insights into deformation and fluid flow processes in the Nankai Trough accretionary prism: Results of Ocean Drilling Program Leg 190: Geochemistry Geophysics Geosystems, v. 2, 1058, https://doi.org/10.1029/2001GC000166.

Moore, J.C., Biju-Duval, B., Bergen, J.A., Blackington, G., Claypool, G.E., Cowan, D.S., Duennebier, F., Guerra, R.T., Hemleben, C.H.J., Hussong, D., Marlow, M.S., Natland, J.H., Pudsey, C.J., Renz, G.W., Tardy, M., Willis, M.E., Wilson, D., and Wright, A.A., 1982, Offscraping and underthrusting of sediment at the deformation front of the Barbados Ridge: Deep Sea Drilling Project Leg 78A: Geological Society of America Bulletin, v. 93, no. 11, p. 1065–1077, https://doi.org/10.1130/0016-7606(1982)93<1065:OAUOSA>2.0.CO;2.

Moran, K., Bruckmann, W., Feeser, V., and Campanella, R.G., 1993, In situ stress conditions at Nankai Trough, Site 808, *in* Hill, I.A., Taira, A., Firth, J.V., et al., Proceedings of the Ocean Drilling Program, Scientific Results, Volume 131: College Station, Texas, Ocean Drilling Program, p. 282–291.

Morgan, J., and Karig, D., 1995, Kinematics and a balanced and restored cross-section across the toe of the eastern Nankai accretionary prism: Journal of Structural Geology, v. 17, no. 1, p. 31–45, https://doi.org/10.1016/0191-8141(94)E0031-S.

Morgan, J.K., Karig, D.E., and Maniatty, A., 1994, The estimation of diffuse strains in the toe of the western Nankai accretionary prism: A kinematic solution: Journal of Geophysical Research: Solid Earth, v. 99, no. B4, p. 7019–7032, https://doi.org/10.1029/93JB03367.

Morgan, J.K., Ramsey, E.B., and Ask, M.V., 2007, Deformation and mechanical strength of sediments at the Nankai subduction zone, *in* Dixon, T.H., and Moore, J.C., eds., The Seismogenic Zone of Subduction Thrust Faults: New York, Columbia University Press, p. 210–256, https://doi.org/10.7312/dixo13866.

Mountney, N., and Westbrook, G., 1996, Modelling sedimentation in ocean trenches: The Nankai Trough from 1 Ma to present: Basin Research, v. 8, p. 85–101, https://doi.org/10.1111/j.1365-2117.1996.tb00116.x.

Nakanishi, A., Takahashi, N., Yamamoto, Y., Takahashi, T., Citak, S.O., Nakamura, T., Obana, K., Kodaira, S., and Kaneda, Y., 2018, Three-dimensional plate geometry and P-wave velocity models of the subduction zone in SW Japan: Implications for seismogenesis, *in* Byrne, T., Underwood, M.B., Fisher, D., McNeill, L., Saffer, D., Ujiie, K., and Yamaguchi, A., eds., Geology and Tectonics of Subduction Zones: A Tribute to Gaku Kimura: Geological Society of America Special Paper 534, p. 69–86, https://doi.org/10.1130/2018.2534(04).

Okino, K., Shimakawa, Y., and Nagaoka, S., 1994, Evolution of the Shikoku Basin: Journal of Geomagnetism and Geoelectricity, v. 46, no. 6, p. 463–479, https://doi.org/10.5636/jgg.46.463.

Olsen, K.M., Bangs, N.L., Tréhu, A.M., Han, S., Arnulf, A., and Contreras-Reyes, E., 2020, Thick, strong sediment subduction along south-central Chile and its role in great earthquakes: Earth and Planetary Science Letters, v. 538, p. 116–195, https://doi.org/10.1016/j.epsl.2020.116195.

Park, J.O., Naruse, H., and Bangs, N.L., 2014, Along strike variations in the Nankai shallow décollement properties and their implications for tsunami earthquake generation: Geophysical Research Letters, v. 41, p. 7057–7064, https://doi.org/10.1002/2014GL061096.

Pedley, K.L., Barnes, P.M., Pettinga, J.R., and Lewis, K.B., 2010, Seafloor structural geomorphic evolution of the accretionary frontal wedge in response to seamount subduction, Poverty Indentation, New Zealand: Marine Geology, v. 270, no. 1–4, p. 119–138, https://doi.org/10.1016/j.margeo.2009.11.006.

Pickering, K.T., Underwood, M.B., and Taira, A., 1992, Open-ocean to trench turbidity-current flow in the Nankai Trough: Flow collapse and reflection: Geology, v. 20, no. 12, p. 1099–1102, https://doi.org/10.1130/0091-7613(1992)020<1099:OOTTTC>2.3.CO;2.

Pickering, K.T., Underwood, M.B., and Taira, A., 1993, Stratigraphic synthesis of the DSDP-ODP sites in the Shikoku Basin, Nankai Trough and accretionary prism, *in* Hill, I.A., Taira, A., Firth, J.V., et

al., Proceedings of the Ocean Drilling Program: Scientific Results, Volume 131: College Station, Texas, Ocean Drilling Program, p. 313–330, https://doi.org/10.2973/odp.proc.sr.131.135.1993.
Pickering, K.T., Underwood, M.B., Saito, S., Naruse, H., Kutterolf, S., Scudder, R., Park, J.-O., Moore, G.F., and Slagle, A., 2013, Depositional architecture, provenance, and tectonic/eustatic modulation of Miocene submarine fans in the Shikoku Basin: Results from Nankai Trough Seismogenic Zone Experiment: Geochemistry Geophysics Geosystems, v. 14, no. 6, p. 1722–1739, https://doi.org/10.1002/ggge.20107.
Plaza-Faverola, A., Klaeschen, D., Barnes, P., Pecher, I., Henrys, S., and Mountjoy, J., 2012, Evolution of fluid expulsion and concentrated hydrate zones across the southern Hikurangi subduction margin, New Zealand: An analysis from depth migrated seismic data: Geochemistry Geophysics Geosystems, v. 13, Q08018, https://doi.org/10.1029/2012GC004228.
Saffer, D.M., 2010, Hydrostratigraphy as a control on subduction zone mechanics through its effects on drainage: An example from the Nankai margin, SW Japan: Geofluids, v. 10, p. 114–131, https://doi.org/10.1111/j.1468-8123.2009.00276.x.
Saffer, D.M., and Bekins, B.A., 2002, Hydrologic controls on the morphology and mechanics of accretionary wedges: Geology, v. 30, no. 3, p. 271–274, https://doi.org/10.1130/0091-7613(2002)030<0271:HCOTMA>2.0.CO;2.
Sato, H., Machida, S., Kanayama, S., Taniguchi, H., and Ishii, T., 2002, Geochemical and isotopic characteristics of the Kinan Seamount Chain in the Shikoku Basin: Geochemical Journal, v. 36, p. 519–526, https://doi.org/10.2343/geochemj.36.519.
Schueller, S., Braathen, A., Fossen, H., and Tveranger, J., 2013, Spatial distribution of deformation bands in damage zones of extensional faults in porous sandstones: Statistical analysis of field data: Journal of Structural Geology, v. 52, p. 148–162, https://doi.org/10.1016/j.jsg.2013.03.013.
Sdrolias, M., Roest, W.R., and Müller, R.D., 2004, An expression of Philippine Sea plate rotation: The Parece Vela and Shikoku basins: Tectonophysics, v. 394, p. 69–86, https://doi.org/10.1016/j.tecto.2004.07.061.
Shipton, Z.K., and Cowie, P.A., 2003, A conceptual model for the origin of fault damage zone structures in high-porosity sandstone: Journal of Structural Geology, v. 25, no. 3, p. 333–344, https://doi.org/10.1016/S0191-8141(02)00037-8.
Steurer, J.F., and Underwood, M.B., 2003, Clay mineralogy of mudstones from the Nankai Trough reference sites and frontal accretionary prism, *in* Mikada, H., Moore, G.F., Taira, A., Becker, K., Moore, J.C., Klaus, A., et al., Proceedings of the Ocean Drilling Program, Scientific Results, Volume 190/196: College Station, Texas, Ocean Drilling Program, p. 1–37, https://doi.org/10.2973/odp.proc.sr.190196.211.2003.
Sun, T., Saffer, D., and Ellis, S., 2020, Mechanical and hydrological effects of seamount subduction on megathrust stress and slip: Nature Geoscience, v. 13, no. 3, p. 249–255, https://doi.org/10.1038/s41561-020-0542-0.
Suppe, J., 1983, Geometry and kinematics of fault-bend folding: American Journal of Science, v. 283, p. 684–721, https://doi.org/10.2475/ajs.283.7.684.
Suppe, J., and Medwedeff, D.A., 1990, Geometry and kinematics of fault-propagation folding: Eclogae Geologicae Helvetiae, v. 83, p. 409–454.
Taira, A., Hill, I.A., Firth, J., et al., 1991, Proceedings of the Ocean Drilling Program, Initial Reports, Volume 131: College Station, Texas, Ocean Drilling Program, 531 p.
Taylor, B., and Fujioka, K., 1992, Rifting and the volcanic-tectonic evolution of the Izu-Bonin-Mariana arc, *in* Taylor, B., Fujioka, K., et al., Proceedings of the Ocean Drilling Program, Scientific Results, Volume 126: College Station, Texas, Ocean Drilling Program, p. 627–651.
Thomas, W.A., 1977, Evolution of Appalachian-Ouachita salients and recesses from reentrants and promontories in the continental margin: American Journal of Science, v. 277, no. 10, p. 1233–1278, https://doi.org/10.2475/ajs.277.10.1233.
Ujiie, K., Maltman, A.J., and Sánchez-Gómez, M., 2004, Origin of deformation bands in argillaceous sediments at the toe of the Nankai accretionary prism, southwest Japan: Journal of Structural Geology, v. 26, no. 2, p. 221–231, https://doi.org/10.1016/j.jsg.2003.06.001.
Underwood, M.B., 2007, Sediment inputs to subduction zones: Why lithostratigraphy and clay mineralogy matter, *in* Dixon T., and Moore, J.C., eds., The Seismogenic Zone of Subduction Thrust Faults: New York, Columbia University Press, p. 42–85, https://doi.org/10.7312/dixo13866.
Underwood, M.B., and Fergusson, C.L., 2005, Late Cenozoic evolution of the Nankai trench-slope system: Evidence from sand petrography and clay mineralogy, *in* Hodgson, D.M., and Flint, S.S., eds., Submarine Slope Systems: Processes and Products: Geological Society [London] Special Publication 244, p. 113–129, https://doi.org/10.1144/GSL.SP.2005.244.01.07.
Underwood, M.B., and Pickering, K.T., 2018, Facies architecture, detrital provenance, and tectonic modulation of sedimentation in the Shikoku Basin: Inputs to the Nankai Trough subduction zone, *in* Byrne, T., Underwood, M.B., Fisher, D., McNeill, L., Saffer, D., Ujiie, K., and Yamaguchi, A., eds., Geology and Tectonics of Subduction Zones: A Tribute to Gaku Kimura: Geological Society of America Special Paper 534, p. 1–34, https://doi.org/10.1130/2018.2534(01).
Underwood, M.B., Saito, S., Kubo, Y., and the Expedition 322 Scientists, 2010, Expedition 322 summary, *in* Saito, S., Underwood, M.B., Kubo, Y., and the Expedition 322 Scientists, Proceedings of the Integrated Ocean Drilling Program, Volume 322: Tokyo, Japan, Integrated Ocean Drilling Program Management International, Inc., https://doi.org/10.2204/iodp.proc.322.101.2010.
Vidal-Royo, O., Koyi, H.A., and Muñoz, J.A., 2009, Formation of orogen-perpendicular thrusts due to mechanical contrasts in the basal décollement in the Central External Sierras (southern Pyrenees, Spain): Journal of Structural Geology, v. 31, no. 5, p. 523–539, https://doi.org/10.1016/j.jsg.2009.03.011.
von Huene, R., Klaeschen, D., Gutscher, M., and Fruehn, J., 1998, Mass and fluid flux during accretion at the Alaskan margin: Geological Society of America Bulletin, v. 110, no. 4, p. 468–482, https://doi.org/10.1130/0016-7606(1998)110<0468:MAFFDA>2.3.CO;2.
von Huene, R., Miller, J.J., and Weinrebe, W., 2012, Subducting plate geology in three great earthquake ruptures of the western Alaska margin, Kodiak to Unimak: Geosphere, v. 8, no. 3, p. 628–644, https://doi.org/10.1130/GES00715.1.
Wang, C.-y., Hwang, W.-t., and Cochrane, G.R., 1994, Tectonic dewatering and mechanics of protothrust zones: Example from the Cascadia accretionary margin: Journal of Geophysical Research: Solid Earth, v. 99, no. B10, p. 20043–20050, https://doi.org/10.1029/94JB01545.
Watts, A., and Weissel, J., 1975, Tectonic history of the Shikoku marginal basin: Earth and Planetary Science Letters, v. 25, no. 3, p. 239–250, https://doi.org/10.1016/0012-821X(75)90238-1.
Weiss, J.R., Ito, G., Brooks, B.A., Olive, J.-A., Moore, G.F., and Foster, J.H., 2018, Formation of the frontal thrust zone of accretionary wedges: Earth and Planetary Science Letters, v. 495, p. 87–100, https://doi.org/10.1016/j.epsl.2018.05.010.
Wu, J., Suppe, J., Lu, R., and Kanda, R., 2016, Philippine Sea and East Asian plate tectonics since 52 Ma constrained by new subducted slab reconstruction methods: Journal of Geophysical Research: Solid Earth, v. 121, no. 6, p. 4670–4741, https://doi.org/10.1002/2016JB012923.
Yamashita, M., Miura, S., Moore, G.F., Nakanishi, A., Kodaira, S., and Kaneda, Y., 2018, Bathymetric imaging of protothrust zone along the Nankai Trough: The Island Arc, v. 27, e12233, https://doi.org/10.1111/iar.12233.